Science of the Total Environment 409 (2011) 2163–2178

Contents lists available at ScienceDirect

Science of the Total Environment

journal homepage: www.elsevier.com/locate/scitotenv

An annual assessment of air quality with the CALIOPE modeling system over Spain

J.M. Baldasano [a,b,*], M.T. Pay [a], O. Jorba [a], S. Gassó [a,b], P. Jiménez-Guerrero [c]

[a] Earth Sciences Department, Barcelona Supercomputing Center. Barcelona, Spain
[b] Environmental Modeling Laboratory, Technical University of Catalonia, Barcelona, Spain
[c] Department of Physics, University of Murcia, Murcia, Spain

ARTICLE INFO

Article history:
Received 7 September 2010
Received in revised form 20 January 2011
Accepted 21 January 2011
Available online 5 March 2011

Keywords:
Model evaluation
Air quality
Spain
High resolution
O_3 exceedances

ABSTRACT

The CALIOPE project, funded by the Spanish Ministry of the Environment, aims at establishing an air quality forecasting system for Spain. With this goal, CALIOPE modeling system was developed and applied with high resolution (4 km × 4 km, 1 h) using the HERMES emission model (including emissions of resuspended particles from paved roads) specifically built up for Spain. The present study provides an evaluation and the assessment of the modeling system, coupling WRF-ARW/HERMES/CMAQ/BSC-DREAM8b for a full-year simulation in 2004 over Spain. The evaluation focuses on the capability of the model to reproduce the temporal and spatial distribution of gas phase species (NO_2, O_3, and SO_2) and particulate matter (PM10) against ground-based measurements from the Spanish air quality monitoring network. The evaluation of the modeling results on an hourly basis shows a strong dependency of the performance of the model on the type of environment (urban, suburban and rural) and the dominant emission sources (traffic, industrial, and background). The O_3 chemistry is best represented in summer, when mean hourly variability and high peaks are generally well reproduced. The mean normalized error and bias meet the recommendations proposed by the United States Environmental Protection Agency (US-EPA) and the European regulations. Modeled O_3 shows higher performance for urban than for rural stations, especially at traffic stations in large cities, since stations influenced by traffic emissions (i.e., high-NO_x environments) are better characterized with a more pronounced daily variability. NO_x/O_3 chemistry is better represented under non-limited-NO_2 regimes. SO_2 is mainly produced from isolated point sources (power generation and transformation industries) which generate large plumes of high SO_2 concentration affecting the air quality on a local to national scale where the meteorological pattern is crucial. The contribution of mineral dust from the Sahara desert through the BSC-DREAM8b model helps to satisfactorily reproduce episodic high PM10 concentration peaks at background stations. The model assessment indicates that one of the main air quality-related problems in Spain is the high level of O_3. A quarter of the Iberian Peninsula shows more than 30 days exceeding the value 120 μg m^{-3} for the maximum 8-h O_3 concentration as a consequence of the transport of O_3 precursors downwind to/from the Madrid and Barcelona metropolitan areas, and industrial areas and cities in the Mediterranean coast.

1. Introduction

In Europe, human health issues caused by degraded air quality have been extensively studied (Brunekreef and Holgate, 2002; Gryparis et al., 2004; Pénard-Morand et al., 2005) and have motivated the increase of monitoring infrastructures and modeling capabilities. In this sense, the European Commission (EC) and the U.S. Environmental Protection Agency (US-EPA), among others, have shown a great interest in air pollution transport and dynamics. Both entities have set ambient air quality standards for acceptable levels of O_3 (US-EPA, 1991; European Commission, 2008), NO_2, SO_2, PM2.5 and PM10 in ambient air. According to the European regulations (European Commission, 2008), local to regional air quality models are useful tools to assess and understand the dynamics of air pollutants, to forecast the air quality, and to develop emission abatement plans and alert the population when health-related issues occur.

Air pollution limit values and allowed numbers of exceedances established by the European Commission (2008) are still exceeded in the atmospheric boundary layer in Europe and, particularly, in Spain (de Leeuw and Vixseboxse, 2010). Despite improvements due to European legislations, particulate matter and ground-level ozone remain important pollutants affecting human health (EEA, 2009a, b, 2010). The impact of these European policies on the pollutant levels was assessed by the Clean Air for Europe (CAFE) program (Amann et al., 2004; Cuvelier et al., 2007).

The CALIOPE project, funded by the Spanish Ministry of the Environment (Ministerio de Medio Ambiente y Medio Rural y Marino), aims at establishing an air quality forecasting system for Spain

* Corresponding author at: Earth Science Department, Barcelona Supercomputing Center-Centro Nacional de Supercomputación (BSC-CNS), Jordi Girona 29, Edificio Nexus II, 08034 Barcelona, Spain. Tel.: +34 93 413 77 19; fax: +34 93 413 77 21.
E-mail address: jose.baldasano@bsc.es (J.M. Baldasano).

0048-9697/$ – see front matter © 2011 Elsevier B.V. All rights reserved.
doi:10.1016/j.scitotenv.2011.01.041

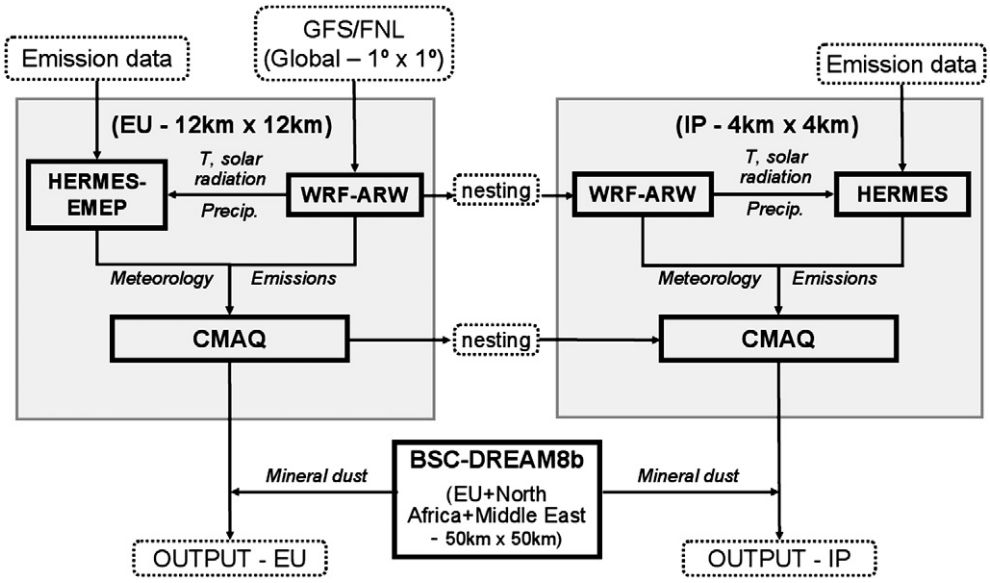

Fig. 1. Modular structure of the CALIOPE modeling system used to simulate air quality dynamics in Spain. Squared boxes with solid lines represent the main models of the framework. Boxes with dashed lines represent input/output dataset. Lines connecting boxes represent the information flow.

(Baldasano et al., 2008a). CALIOPE (Fig. 1) encompasses a high-resolution air quality forecasting system, namely WRF-ARW/HERMES-EMEP/CMAQ/BSC-DREAM8b, being applied to Europe as a mother domain: 12 km × 12 km, 1 h (Pay et al., 2010a) as well as to Spain as the nested domain: 4 km × 4 km,1 h. Such high resolution of the modeling system is made possible by its implementation on the MareNostrum supercomputer hosted by the Barcelona Supercomputing Center-Centro Nacional de Supercomputación (BSC-CNS). Four Spanish research institutes compose the CALIOPE project: the BSC-CNS, the "Centro de Investigaciones Energéticas, Medioambientales y Tecnológicas" (CIEMAT), the Institute of Earth Sciences Jaume Almera of the "Centro Superior de Investigaciones Científicas "(IJA-CSIC) and the "Centro de Estudios Ambientales del Mediterráneo" (CEAM). In this project both experimental and operational modeling aspects are conducted by the BSC-CNS and CIEMAT while IJA-CSIC and CEAM lead the data monitoring part for the evaluation processes. Current forecasts are available through http://www.bsc.es/caliope.

To date, a total of 23 model systems routinely simulate the air quality over Europe, with seven systems also operated in the forecasting mode (Menut and Bessagnet, 2010). Due to the episodic nature of dust outbreaks, the representation of these events cannot be well simulated with solely the information of aerosol boundary conditions (Jiménez-Guerrero et al., 2008a; Menut and Bessagnet, 2010). Vautard et al. (2005a) showed that simulated aerosol loadings, using the current knowledge on aerosol mechanisms, may be underestimated by up to 30–50% if only anthropogenic sources are taken into account. Among the seven operational systems CALIOPE is the unique system including the contribution of Saharan dust on an hourly basis. In addition, CALIOPE includes the High-elective Resolution Modelling Emission System (HERMES, see Baldasano et al., 2008b) specifically applied with high resolution over Spain.

Several studies investigated air quality concerns over selected areas in Spain (San José et al., 1999; Jiménez-Guerrero et al., 2008b; Vivanco et al., 2008) or over the entire Peninsula (Baldasano et al., 2008a; Jiménez-Guerrero et al., 2008a; Vivanco et al., 2009). Most models ran with horizontal cell resolution of 18 km × 18 km or coarser for domains covering the Spanish territory. CALIOPE now uses a 4 km × 4 km cell resolution to simulate the Iberian Peninsula domain. Such high resolution is a key factor to accurately simulate air pollution issues, especially over complex topography (Jiménez et al., 2006) and meteorology patterns (Baldasano et al., 1994; Millán et al., 2002) in southern Europe.

The present paper provides a quantitative performance assessment of the CALIOPE modeling system to simulate the air quality in Spain (gas phase and particulate matter). As the HERMES emission database was compiled for the year 2004 the evaluation was carried out over this year. The performance of the modeling system is evaluated by means of comparisons with ground-based observations from the Spanish network hereinafter referred to as "RedESP" (source: CEAM, see Fig. 2). The model dynamics are evaluated together with the corresponding statistics. The results are then compared to model performance goals and criteria. This study intends to warrant the suitability of CALIOPE over Spain for air quality concerns and forecast.

Section 2 describes the different models used in the CALIOPE system, the observational dataset and the statistical parameters calculated. Section 3 analyzes the results against available observations for the year 2004 and the modeled annual distribution of NO_2, O_3, SO_2 and PM10. A discussion about the exceedances of O_3 during summertime is shown in Section 4. The conclusions are drawn in Section 5.

2. Methods

2.1. System Description

The CALIOPE air quality system is a state-of-the-art modeling framework. As shown in Fig. 1, CALIOPE is a complex system that integrates the meteorological model: WRF-ARW, the emission model: HERMES, the chemical transport model: CMAQ, and the mineral dust atmospheric model: BSC-DREAM8b offline coupled in an air quality forecasting system (Baldasano et al., 2008a).

The Advanced Research Weather Research and Forecasting (WRF-ARW) model v3.0.1.1 (Michalakes et al., 2004; Skamarock and Klemp, 2008) provides the meteorology fields required by the chemical transport model. For the Spanish domain WRF-ARW is configured with a grid of 397 × 397 points corresponding to a 4 km × 4 km horizontal resolution and 38 σ vertical levels with 11 characterizing the planetary boundary layer (PBL). The model top is defined at 50 hPa to resolve the troposphere–stratosphere exchanges properly. Details

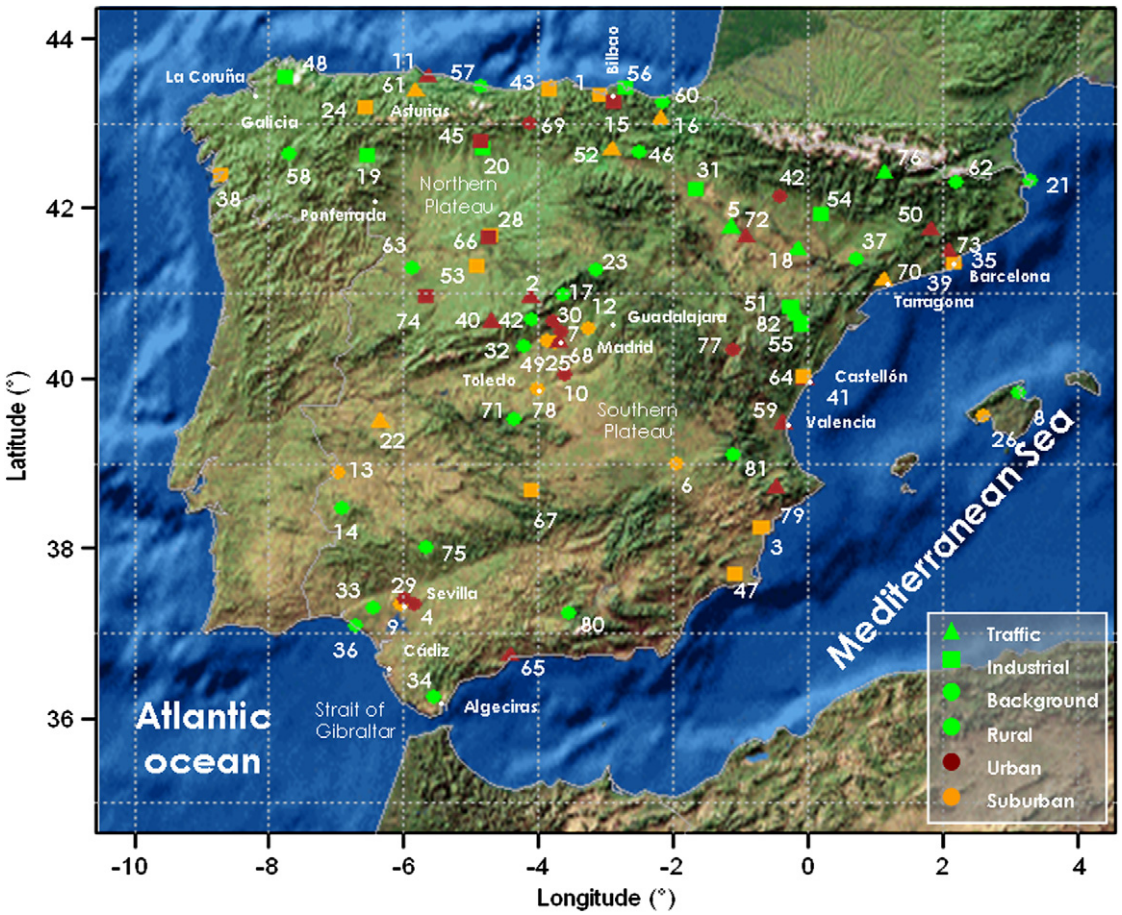

Fig. 2. RedESP stations measuring air pollutants in Spain on an hourly basis in 2004. Different types of stations (U: Urban; S: Suburban; R: Rural; B: Background; I: Industrial; and T: Traffic) according to Garber et al. (2002) are represented by symbols and color codes. The various symbols represent the major emission types affecting each station (Traffic: triangle; Industrial: square; and Background: circle) while the colors reflect the environment of each station (Urban: red; Suburban: green; and Rural: orange). Characteristics and number of each station are listed in Table 1.

about the performance of WRF-ARW over the Spanish domain are provided as supplementary material.

The Models-3 Community Multiscale Air Quality Modeling System (Models-3/CMAQ, Byun and Ching, 1999; Binkowski, 1999; Byun and Schere, 2006), v4.5 is used to study the behavior of air pollutants from regional to local scales, due to its generalized coordinate system and its advanced nesting grid capability. It includes gas, aerosol and heterogeneous chemistry. According to the work by Jiménez et al. (2003) the gas-phase chemistry mechanism used in this study is the Carbon Bond IV (CBM-IV, Gery et al., 1989). The version of CBM-IV mechanism is that presented in CMAQv4.5 original code (Appel et al., 2007, 2008) which introduces some changes and updates in the original CBM-IV mechanism such as an update isoprene chemistry to Carter's one product form (Carter, 2000) and an inclusion of gaseous species that are necessary to link gas-phase chemistry to aerosol formation.

The aerosols are modeled using the AERO4 module (Binkowski and Roselle, 2003). This module comprises the following aerosol components: nitrate, sulfate, ammonium, elemental and organic carbon (with three subcomponents: primary, secondary anthropogenic and secondary biogenic), soil, sodium, and chlorine. Unspecified anthropogenic aerosols and aerosol water are additionally kept as separate components. Aerosols are represented by a three size modes (Aitken, accumulation and coarse mode) each of them assumed to have a lognormal distribution. The coarse particles mode is treated as dry and chemically inert with a fixed geometric standard deviation of 2.2 (Kelly et al., 2010), thus there is no dynamic interaction between the fine and coarse mode. The production of sea salt aerosol (SSA) is implemented as a function of wind speed and relative humidity (Gong, 2003; Zhang et al., 2005) through the AERO4 aerosol module.

Secondary inorganic aerosols (SIA) are generated by nucleation processes from their precursors to form nitrate ammonium and sulfate aerosols. The thermodynamic equilibrium between gas and inorganic fine aerosols is determined by the ISORROPIA model (Nenes et al., 1998). Secondary Organic Aerosols (SOA) are simulated following a traditional 2-product SOA model (Binkowski and Roselle, 2003) where SOA concentrations are yield from the oxidation of six primary organic gases: alkanes, alkenes, cresol, high-yield aromatics, low yield aromatics, and monoterpenes. Ten semi-volatile organic compounds are produced via these reactions—two each for olefins, monoterpenes, and aromatics, and one each for alkanes and cresol. The oxidants include the hydroxyl radical, the nitrate radicals, and ozone. The saturation vapor pressures and mass-based stoichiometric yield coefficients of semi-volatile organic compounds are obtained from either smog chamber experiments or from published estimates in cases where smog chamber data are unavailable. The SOA is calculated using the method developed by Schell et al. (2001) and gas and aerosol-phase concentrations of each semi-volatile organic compounds are calculated iteratively using a globally convergent variation of Newton's method. The formation rates of aerosol mass (in terms of the reaction rates of the precursors) are taken from Pandis et al. (1992).

Aerosol deposition is treated by a second-generation deposition velocity scheme (Binkowski and Shankar, 1995; Venkatram and

Table 1
Location and characteristics of selected RedESP stations (source: CEAM) for 2004 on an hourly basis. 68 Stations were used to monitor NO_2, 45 for SO_2, 82 for O_3, and 44 for PM10, respectively.

	Station name	Latitude[a]	Longitude[a]	Altitude (m)	Type[b]	Hourly concentration			
						NO_2	SO_2	O_3	PM10
1	Abanto	+43.322	−3.073	75	SI	x	x	x	x
2	Acueducto	+40.950	−4.116	1002	UT	x		x	x
3	Agro	+38.242	−0.683	44	SI	x	x	x	
4	Al. Guadaira	+37.342	−5.833	68	UB	x		x	x
5	Alagón	+41.763	−1.143	235	RT	x	x	x	
6	Albacete	+38.981	−1.957	686	SB	x	x	x	x
7	Alcobendas(R.)	+40.541	−3.646	688	UB	x	x	x	x
8	Alcudial − Alc	+39.838	+3.147	15	RB	x		x	
9	Aljarafe	+37.340	−6.043	68	SB	x	x	x	x
10	Aranjuez	+40.034	−3.592	501	UB	x		x	x
11	Av. Castilla	+43.538	−5.646	7	UT	x	x	x	x
12	Azuqueca	+40.574	−3.263	662	SB	x	x	x	x
13	Badajoz	+38.892	−6.970	390	SB	x		x	x
14	Barcarrota	+38.476	−6.923	393	RB	x	x	x	
15	Basauri	+43.240	−2.881	125	UI	x	x	x	x
16	Beasain	+43.048	−2.191	153	ST	x		x	x
17	Buitrago	+40.979	−3.622	1024	RB			x	
18	Bujaralo	+41.505	−0.152	327	RT	x		x	
19	C.T. Compos1	+42.626	−6.521	720	RI	x		x	x
20	C.T. Guardo2	+42.704	−4.827	1065	RI			x	
21	Cabo de Creus	+42.319	+3.316	23	RB	x	x	x	
22	Cáceres	+39.482	−6.357	389	ST	x		x	x
23	Campisábalos	+41.281	−3.143	1360	RB	x	x	x	
24	Cangas	+43.181	−6.550	330	SI	x	x	x	x
25	Casa Campo	+40.420	−3.750	645	SB	x		x	x
26	Cast. Bellver	+39.564	+2.623	117	SB	x	x	x	x
27	Castellón	+39.983	−0.045	28	UT	x	x	x	x
28	Cementerio	+41.674	−4.697	695	SI	x		x	
29	Centro	+37.389	−5.992	19	UB			x	
30	Colmenar	+40.665	−3.774	905	UB	x		x	x
31	CTCC−Arguedas	+42.225	−1.667	490	RI	x	x	x	x
32	Chapinería	+40.378	−4.205	675	RB	x		x	x
33	Doñana	+37.285	−6.440	20	RB	x		x	x
34	E2 Alcornocales	+36.234	−5.540	189	RB			x	
35	Eixample	+41.386	+2.154	12	UT	x	x	x	
36	El Arenosillo	+37.088	−6.705	37	RB			x	
37	Els Torm	+41.395	+0.721	470	RB	x	x	x	
38	Esc. Naval	+42.395	−8.708	20	SI		x	x	
39	Escullera	+41.353	+2.177	16	SI			x	
40	Estación	+40.657	−4.690	1150	UT	x		x	x
41	Grao	+39.984	+0.009	10	SI	x	x	x	
42	Guadarra	+40.679	−4.105	1025	RB			x	
43	Guarnizo	+43.404	−3.842	16	SI	x	x	x	x
44	Huesca	+42.136	−0.404	488	UB			x	
45	Instituto	+42.792	−4.847	1120	UI	x	x	x	x
46	Izkiz	+42.653	−2.501	810	RB	x	x	x	x
47	La Aljorra	+37.694	−1.068	80	SI	x		x	x
48	Louseiras	+43.536	−7.740	540	RI	x	x	x	x
49	Majadahonda	+40.446	−3.868	730	SB	x		x	x
50	Manresa	+41.731	1.826	238	UT	x		x	
51	Mas Matas	+40.841	−0.249	510	RI	x	x	x	x
52	Mda. de Ebro1	+42.682	−2.918	471	ST			x	
53	Medina	+41.316	−4.909	721	SI	x		x	x
54	Monzón	+41.918	+0.197	279	RI			x	
55	Morella	+40.636	−0.093	1150	RI	x	x	x	x
56	Mundaka	+43.406	−2.704	116	RI	x	x	x	x
57	Niembro	+43.439	−4.850	134	RB	x	x	x	
58	O Saviñao	+42.635	−7.705	506	RB	x	x	x	
59	P. Silla	+39.458	−0.377	11	UT	x	x	x	
60	Pagoeta	+43.251	−2.155	215	RB	x		x	x
61	Pal. Deportes	+43.367	−5.831	206	ST	x	x	x	x
62	Pardines	+42.312	+2.214	1224	RB		x	x	
63	Penausende	+41.289	−5.867	985	RB	x	x	x	
64	Peneta	+40.013	−0.058	106	SI	x	x	x	
65	Ps. Martiricos	+36.729	−4.427	4	UT	x		x	x
66	Pte. Regeral	+41.654	−4.735	691	UI	x	x	x	x
67	Puertollano	+38.683	−4.089	670	SI	x	x	x	x
68	Recoletos	+40.423	−3.692	648	UT	x	x	x	x
69	Reinosa	+43.001	−4.136	851	UB	x	x	x	x
70	Reus	+41.151	+1.120	103	ST	x	x	x	
71	Risco Llano	+39.523	−4.353	1241	RB	x	x	x	
72	Roger Flor	+41.651	−0.917	212	UT	x		x	x
73	S. Cugat	+41.481	+2.090	113	UT	x	x	x	

Table 1 (*continued*)

	Station name	Latitude[a]	Longitude[a]	Altitude (m)	Type[b]	Hourly concentration			
						NO_2	SO_2	O_3	PM10
74	Salamanca2	+40.965	−5.656	797	UI	x	x	x	
75	Sierra Norte	+37.996	−5.666	569	RB	x		x	x
76	Sort	+42.407	+1.130	692	RT		x	x	
77	Teruel	+40.336	−1.107	915	UB			x	
78	Toledo	+39.867	−4.021	500	SB	x		x	x
79	Verge	+38.707	−0.467	534	UT	x	x	x	
80	Víznar	+37.237	−3.534	1230	RB	x	x	x	
81	Zarra	+39.086	−1.102	885	RB	x	x	x	
82	Zorita	+40.734	−0.169	619	RB	x	x	x	x

[a] A positive value indicates northern latitudes or eastern longitudes. A negative value indicates southern latitudes or western longitudes.
[b] U: Urban; S: Suburban; R: Rural; B: Background; I: Industrial; T: Traffic. See Garber et al. (2002).

Pleim, 1999). For a more complete description of the processes implemented in CMAQ see Byun and Schere (2006).

The CMAQ horizontal grid resolution corresponds to that of WRF. Its vertical structure was obtained by a collapse from the 38 WRF layers to a total of 15 layers steadily increasing from the surface up to 50 hPa with a stronger density within the PBL.

In order to provide adequate boundary and initial conditions to the IP domain the CALIOPE modeling system was initially run on a regional scale (12 km × 12 km in space and 1 h in time) to model the European domain (mother domain). Chemical boundary conditions for this domain were provided by the global climate chemistry model LMDz-INCA2 (Hauglustaine et al., 2004; Folberth et al., 2006). A detailed evaluation of the European simulation was recently presented in the companion paper by Pay et al. (2010a). A one-way nesting was then performed to retrieve the meteorological and chemical conditions for the IP domain (see Fig. 1).

As highlighted by Lam and Fu (2009) stratospheric amounts of O_3 interpolated from global chemical models and provided to the chemical lateral profiles may cause problems since CMAQ does not include a cross-tropopause exchange mechanism. Following their suggestion the stratospheric contribution of O_3 from the mother domain was suppressed from the chemical boundary conditions to avoid inconsistent intrusions of stratospheric O_3 down to the surface.

The HERMES model (Baldasano et al., 2008b) uses information and state-of-the-art methodologies for emission estimations. It calculates emissions by sector-specific sources or by individual installations and stacks. Emissions used for Spain are derived from the aggregation in space from 1 km × 1 km dataset to 4 km × 4 km. Raw emission data are processed by HERMES in order to provide a comprehensive description of the emissions to the air quality model. In this study estimated emissions are expressed in CBM-IV speciation.

According to natural emissions, HERMES calculates the biogenic volatile organic compounds (bVOC) from vegetation (Baldasano et al., 2008b). Three categories of bVOC are estimated according to their reactivity: isoprene, monoterpenes and other volatile organic compounds (OVOC). The model considers the influence of temperature and photosynthetically active radiation (PAR) by Guenther et al. (1995) algorithms, according to Parra et al. (2004, 2006). Emission factors for each individual vegetal species associated with emitter land-use categories are presented in Parra et al. (2004). The land-use categories for each grid cell are obtained from CORINE Land Cover 2000 map starting with a resolution of 100 m, and adapting to 22 the land-use categories according to Arévalo et al. (2004). In the updated version of HERMES model used in the present work, the influence of seasonality in the emission of bVOC is introduced through an environmental correction factor following Staudt et al. (2000) y Steinbrecher et al. (2009). In the specific case of bVOC, estimated emissions with the HERMES model are expressed in terms of CBM-IV variables based on profiles in SPECIATE 3.2 (http://www.epa.gov/ttn/chief/emch/speciation/cbiv-profiles_mar_4_2002.xls). Wildfire emissions and NO_x production from soils and lightning are not currently calculated by HERMES model. Wildfires are an important source of atmospheric pollutants (NO_x, volatile organic carbon, particulate matter) on the Iberian Peninsula during the dry season, especially in summertime (European Commission, 2005). The inclusion of aforementioned natural emissions could be an important point to improve in order to better reproduce air quality in Spain during summer.

HERMES was recently updated with the following: inclusion of agriculture and livestock emissions (SNAP10 sector, see Baldasano et al., 2008b), improvement in the spatial distribution of biogenic emission and population density via the use of the Corine Land Cover information at a 100-m resolution, and introduction of emissions from the road traffic sector in small cities (SNAP07 sector).In addition, the current version of HERMES model quantifies particulate emissions resulting from paved road resuspension following the parameterization described in Pay et al. (2010b). The inclusion of resuspended particles from paved road is an important feature for PM10 studies in urban air pollution (Querol et al., 2004b; Amato et al., 2009a,b, 2010).

The Dust REgional Atmospheric Model (BSC-DREAM8b) was designed to simulate and predict the atmospheric cycle of mineral dust (Nickovic et al., 2001; Pérez et al., 2006a,b). The domain considered in this study comprises northern Africa, the Mediterranean basin and Europe. BSC-DREAM8b is fully embedded within the NCEP/Eta meteorological driver (Janjic, 1994). It simulates the long-range transport of mineral dust at a 0.3º × 0.3° resolution using 24 vertical layers extending up to 15 km in altitude on an hourly basis. The aerosol description contains 8 bins to allow a fine description of dust aerosols. Dust–radiation interactions are calculated online.

The BSC-DREAM8b is offline coupling and its outputs are then simply added to the CMAQ-calculated particulate matter (Jiménez-Guerrero et al., 2008a). Since BSC-DREAM8b used a 50 km × 50 km horizontal resolution, its outputs are interpolated to the CMAQ's Lambert conformal conic grid with a 4 km × 4 km horizontal resolution. After the interpolation, total modeled PM10 is the sum of the Aitken, accumulation and coarse species from CMAQ and the corresponding bins with diameter less than and equal to 10 μm. CMAQ internally distributes primary coarse particulate matter emissions into the model species ASOIL and ACORS using a 90%/10% split based on the fact that the US emissions inventory estimates that 90% of PM10 is fugitive dust (Binkowski and Roselle, 2003). In the CALIOPE modeling system the only primary natural dust emissions that are taken into account are those from the Sahara desert included offline through the BSC-DREAM8b model. In this sense, we changed the internal distribution of primary coarse PM emission into the model species ASOIL and ACORS, where all the primary coarse PM emissions are included in ACORS and ASOIL remain near to zero. In this way, only anthropogenic coarse PM emissions (including resuspension from paved-road) are represented in the ACORS variable.

The simulation consists of 366 daily runs constituting the year 2004. The first 12 h of each daily meteorological runs is treated as cold start, and the next 23 h is provided to the chemical transport model via the Meteorology-Chemistry Interface Process from CMAQ (MCIP).

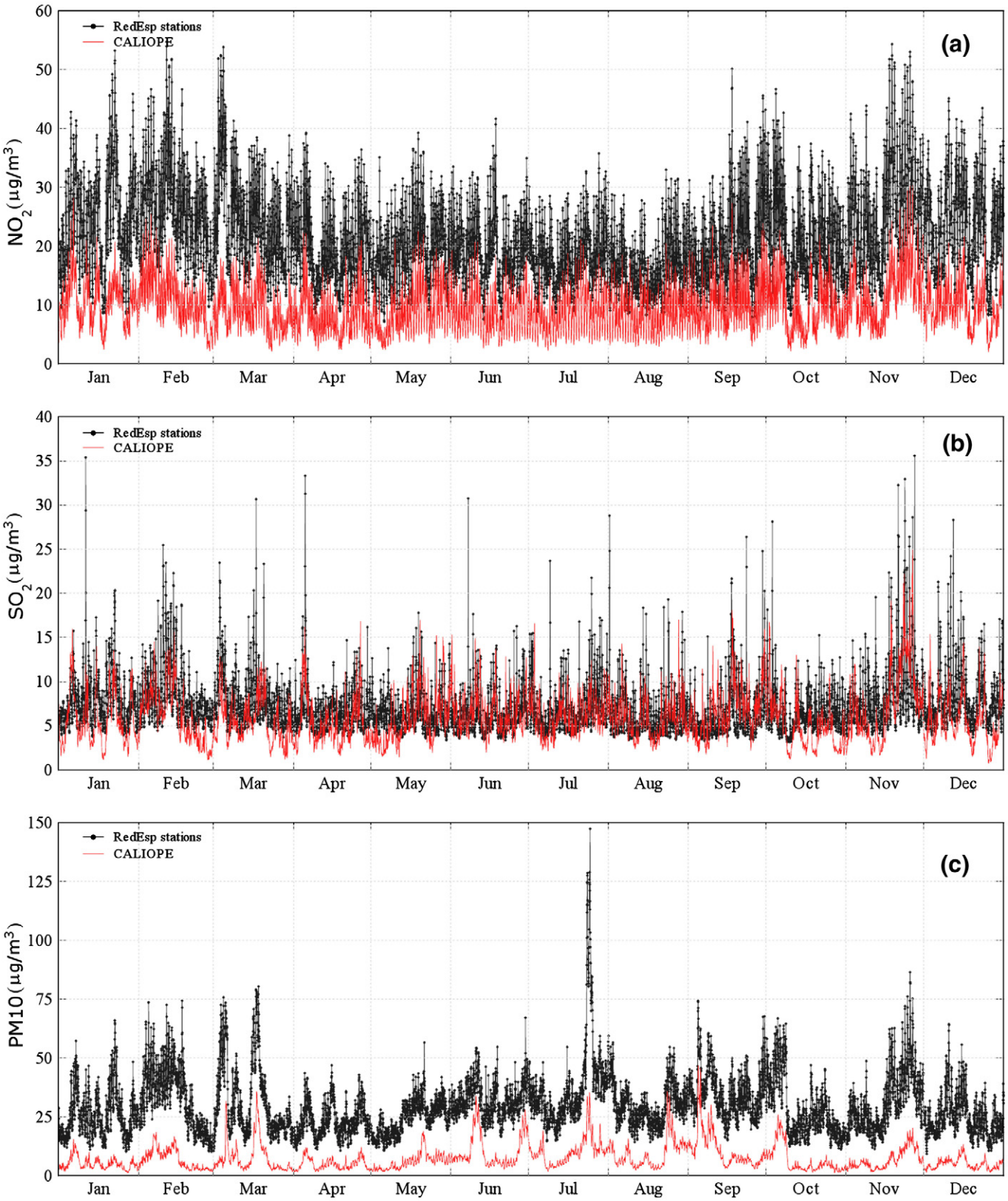

Fig. 3. Modeled (red lines) and measured (marked black lines) time series of hourly mean concentrations (in µg m^{-3}) for NO_2 (a), SO_2 (b) and PM10 (c), respectively, averaged over all the RedESP stations available.

2.2. Air Quality Network

In order to evaluate the performances of the CALIOPE system at ground level over Spain, the hourly data from RedESP Spanish network of air quality monitoring stations were selected. The RedESP network comprises a relatively dense geographical coverage of the Spanish territory. The RedESP observational data provided by CEAM were subject to a preliminary quality control to exclude erroneous

values. Then, all stations with a temporal coverage below 85% of the entire year 2004 were filtered out. The RedESP stations are characterized by the type of environment (urban, suburban and rural) and the dominant emission source (traffic, industrial, and background) based on the proposition by Garber et al. (2002). Characteristics, location and measured pollutants of the RedESP stations are presented in Table 1 and Fig. 2. In summary, a total of 68 measuring stations were used for NO_2, 45 for SO_2, 82 for O_3, and 44 for PM10, respectively.

2.3. Statistical Indicators

A variety of statistical parameters may be used to quantify how well CALIOPE system reproduces the observations (Denby et al., 2010). In particular, specific metrics were proposed depending on the pollutants (US-EPA, 1984, 1991; Cox and Tikvart, 1990; Weil et al., 1992; Chang and Hanna, 2004; Boylan and Russell, 2006).

Common statistical metrics used by the modeling community include the measured and modeled mean, the correlation coefficient (r), the root mean square error (RMSE) and the mean bias (MB). Additionally, the mean normalized bias and gross errors, MNBE and MNGE respectively, considering all modeled/observed pairs of values are also useful parameters. For particulate matter, Boylan and Russell (2006) rather suggested the consideration of the mean fractional bias (MFB) and the mean fractional error (MFE) parameters since they are symmetric metrics, bounding the maximum bias and error.

The US-EPA suggested several performance criteria for simulated O_3, such as MNBE $\leq \pm 15\%$ and MNGE $\leq 35\%$ (US-EPA, 1991, 2007) whereas the EC proposes a modeling quality objective given as a relative uncertainty (%): 50% and 30% for PM10/PM25/O_3 annual average and NO_2/SO_2 annual average, respectively (European Commission, 2008). However, the interpretation of the term model uncertainty remains unclear (Denby et al., 2010). Therefore, the latter criteria will not be further commented in this study. For particulate matter, Boylan and Russell (2006) proposed that the model performance criterion would be met when both MFE $\leq 75\%$ and MFB $\leq \pm$ 60%, respectively, and the model performance goal would be met when MFE and MFB are less than or equal to 50% and $\pm 30\%$, respectively.

The annual mean model-to-data statistics RMSE, correlation coefficient, MNBE, MNGE, MFB and MFE in hourly basis are calculated for the present study. According to the recommendations of the US-EPA a cut-off value of 80 μg m^{-3} was applied to O_3 statistics before compilation (US-EPA, 1991; Russell and Dennis, 2000). However, correlation coefficients for O_3 are calculated without cut-off value in order to test the capability of the model to reproduce the variation of O_3 concentrations.

3. Results and Discussions

First, this section shows a model evaluation through statistical and dynamical performances. Statistics are calculated in hourly basis for NO_2, O_3, SO_2, and PM10. In the case of O_3, the daily peak of hourly O_3 is also computed as it is one of the most important parameters to be considered. Statistics are expressed in annual terms according to different categories: over all stations ("All"), over rural stations ("Rural"), over suburban stations ("Suburban") and over urban stations ("Urban"). Furthermore, a general description of the annual mean distribution of each pollutant is provided to determine each pattern throughout Spain. Note that model outputs are used without any correction factor and the coupling modeling system is used with original codes.

3.1. Nitrogen Dioxide

The NO_2 measurement dataset comprises a relatively equal distribution of station types with 21 urban, 22 suburban and 25 rural stations, respectively. Fig. 3a represents the measured (marked black line) and modeled (red line) time series of the hourly mean NO_2 at the 68 measuring stations. The general modeled dynamics is well captured with a clear signal of the main winter pollution events. However, mean levels of NO_2 are persistently underestimated (MB = -12.3 μg m^{-3}, see Table 2).

The statistics compiled in Table 2 show highest mean RMSE values at urban stations (33.6 μg m^{-3}) and lowest values for rural stations (7.6 μg m^{-3}). This characteristic is not surprising, since urban stations are more likely to be influenced by high, very local emission sources from urban activities which remain difficult to be captured by models. Both MFB and MFE metrics show relatively constant values among the station types, suggesting that the model error for NO_2 is proportional to the normalized observed value. Overall, however, the modeled daily and monthly variations of NO_2 are in good agreement with observations, although a reduced magnitude of the variability is noted. Among the best model behaviors reported, the majority corresponds to either rural stations influenced by background emissions (mean RMSE = 6.3 μg m^{-3} compared to 7.6 μg m^{-3} for all rural stations) or urban stations located in very large (and well characterized) cities such as Madrid or Barcelona (MFB = −46.4% compared to −97.7% for all urban stations). In general, measurements at suburban or urban stations from small- to medium-sized cities were simulated with less accuracy. From the 68 stations measuring NO_2, 13 (19%) were not represented correctly by the model. Most of these stations are placed in small cities and are often located in the vicinity of isolated roads or highways (e.g., Acueducto, Estación, Roger Flor, Verge, Table 1). We attribute such behavior to the incomplete

Table 2
Annual statistics obtained with CALIOPE over Spain for 2004 at the RedESP stations in hourly basis. Statistics are calculated according to four categories: over all stations ("All"), rural stations ("Rural"), suburban stations ("Suburban") and urban stations ("Urban"). Stations/data points column indicates the number of stations (values before slash) and the number of pair measurement-model (values after slash), respectively, used to compute the statistics. The calculated statistics are measured mean (μg m^{-3}), modeled mean (μg m^{-3}), correlation coefficient (r), mean bias (MB, μg m^{-3}), root mean square error (RMSE, μg m^{-3}), mean fractional bias (MFB, %) and error (MFE, %). All metrics are calculated without cut-off value.

Pollutant	Category	Stations/data points	Measured mean	Modeled mean	r	MB	RMSE	MFB	MFE
NO_2 hourly	All	68/552,941	21.6	9.6	0.53	12.3	23.3	−81.1	98.8
	Rural	25/203,606	7.6	3.3	0.51	3.7	7.6	−79.7	95.6
	Suburban	22/178,416	23.2	11.7	0.39	11.5	23.1	−66.7	93.6
	Urban	21/170,919	36.5	14.8	0.47	23.2	33.6	−97.7	107.9
SO_2 hourly	All	45/368,795	7.2	6.1	0.19	0.9	18.7	−33.1	97.8
	Rural	18/150,647	4.4	3.3	0.28	−0.5	14.0	−29.9	94.1
	Suburban	14/110,584	9.1	9.9	0.14	0.6	26.0	−23.8	95.5
	Urban	13/107,564	9.3	6.0	0.14	−3.1	15.1	−47.1	105.4
PM10 hourly	All	44/355,219	29.6	7.5	0.38	−21.8	33.4	−111.8	119.8
	Rural	12/94,873	19.6	5.9	0.43	−11.7	20.4	−96.0	110.4
	Suburban	17/139,479	35.0	8.0	0.36	−27.0	39.7	−118.6	123.6
	Urban	15/120,867	31.8	8.1	0.36	−23.7	33.8	−116.3	122.9

characterization of emissions from small cities and to the influence of the model resolution on sub-grid emission sources. The latter, also known as sub-grid variability, is a well-known issue affecting the results of model-observation comparisons (e.g., Ching et al., 2006). Also, NO_2 concentrations in background areas were found to be systematically underestimated. This trend is supported by the lack of biomass burning (Ortiz de Zárate et al., 2005) and natural NO_x production such as lightnings which are currently not treated in the CALIOPE modeling system (Smith and Mueller, 2010). In addition, biogenic emissions from vegetated and agricultural areas (SNAP10 sector) in HERMES may need further revision.

Fig. 4a displays the annual average modeled levels of NO_2 at lower-most levels over Spain. High concentrations of NO_2 within the PBL are directly related to anthropogenic NO_x emission. Baldasano et al. (2008a) estimated that the largest NO_x emission sources come from combustion in energy and transformation industries (41% of NO_x total emission) followed by road transport (37% of NO_x total emission).

The urban plumes from Madrid and Barcelona metropolitan areas reach the highest NO_2 concentrations (~25–40 μg m^{-3}). In both regions, on-road traffic constitutes the main source of primary pollutants in the region (Gonçalves et al., 2009). In Madrid the NO_2 dispersion follows a south-western direction conditioned by the barrier of Central System (located in the north-western area, 2500 m height) and the canalization of Tajo valley (located in the southern part). The urban plume reaches the highest concentration at the urban nuclei (~40 μg m^{-3}), moving towards Toledo (south) and reaching Guadalajara (east) to a lesser extent. A different NO_2 pattern is observed in Barcelona area. The NO_2 dispersion shows a perpendicular flow to the coast dominated by the north-western winds. The very complex coastal terrain induces mesoscale phenomena which control the superficial wind flows. Sea-breezes and mountain valley winds contribute to the accumulation and recirculation of air masses. The littoral mountain chain (1000–1500 m height) acts as a barrier, recirculating NO_2 flow towards the Mediterranean Sea channeled by the river valleys.

The densely industrialized area of Tarragona and Castellón and the urban area of Valencia, all located along the Mediterranean coast, present significant levels of NO_2 also affected by mesoscale phenomena dominated by sea-breezes which determinate NO_2 flow perpendicular to the coast. In the northern Spain, the urban and industrial areas of Bilbao show significant NO_2 levels (~25 μg m^{-3}) dispersed along an estuary that runs almost 16 km from the center of the city to the sea and is aligned in an SE–NW direction.

In the north-eastern Spain the NO_2 contribution from power plants emission is bigger than the urban contribution, where NO_2 annual mean concentration reaches ~7–15 μg m^{-3} at the ground level.

Due to the high disaggregation and the specifically detailed emissions implemented in the HERMES model, the impact of principal highways is noticeable, (e.g., Madrid-Sevilla, Barcelona-Bilbao, the A-7 Mediterranean highway) where annual mean values range from 3 to 7 μg m^{-3}. Background regions, unaffected by emissions rather have concentrations below 3 μg m^{-3}.

The major shipping route originating from the northern Atlantic and the British Channel, passing along Portugal coast, through the

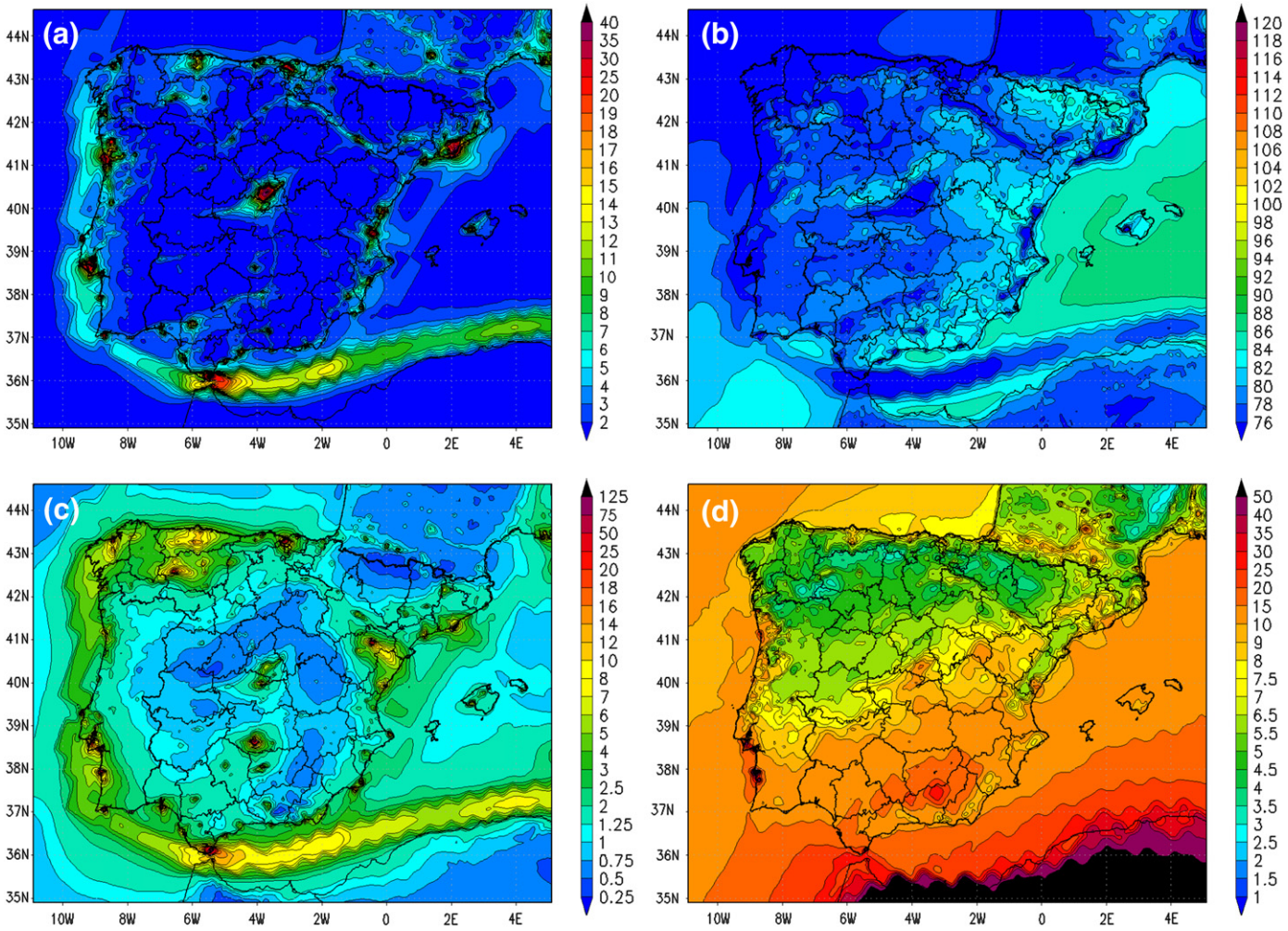

Fig. 4. 2004 Annual average concentrations (μg m^{-3}) of (a) NO_2, (b) O_3, (c) SO_2, and (d) PM10 at lower-most level simulated by CALIOPE over Spain at a 4 km × 4 km spatial resolution.

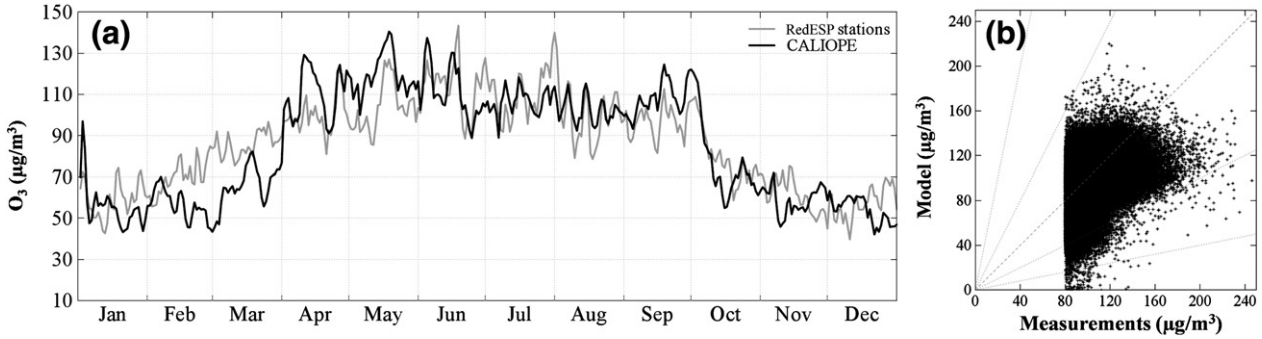

Fig. 5. Modeled (black lines) and measured (grey lines) time series of O_3 daily peak concentrations averaged over the 82 RedESP stations (a) and scatter plots of the O_3 pair measurement model in hourly basis at the 82 RedESP stations (b). The scatter plot includes the 1:1, 1:2, 1:5, and 5:1 reference lines. A cut-off value of 80 μg m^{-3} is applied to the observation in the scatter plot.

Strait of Gibraltar heading toward northern Africa and the Suez Canal is shown to have a notable impact on NO_2 levels. Concentrations of NO_2 range from ~5 μg m^{-3}, near the coastlines of Portugal and Gulf of Cadiz, to ~12 μg m^{-3}, over the Alboran Sea. This difference is accentuated by the distinct Atlantic-Mediterranean regimes of Spain. While in the Mediterranean dynamics in summer are characterized by re-circulation and accumulation of pollutant, a strong dynamically compensated anticyclonic inversion dominates the Spanish Atlantic coast and the west of Portugal (Millán et al., 1997). In the Strait of Gibraltar high NO_2 concentrations are estimated (~30 μg m^{-3}) where three contributions are combined: the maritime traffic and the industrial processes and electric generation developed in the Algeciras area. The complex topography of the Strait induces the NO_2 dispersion aligned in a west to east direction, with generalized strong east wind (Millán et al., 2002).

3.2. Ozone

This study comprises a total of 82 RedESP stations measuring O_3 throughout Spain for the year 2004. 24 Stations are located in urban areas, 25 in suburban zones and 33 in rural areas, respectively. Modeled and measured time series and scatter plot are shown in Fig. 5 with the corresponding statistics in Table 3. Time series for O_3 daily peak (Fig. 5a) show that the O_3 chemistry is best represented in summer. In the high photolytical season, the mean variability and high peaks are generally well reproduced. The modeled variability in winter months is characterized by difficulties to capture the mean trend due to inaccurate description of cross-tropopause exchanges in CMAQ (Pay et al., 2010a). However, the discussion of the evaluation will mainly focus on the high O_3 season (from April to September).

Statistical parameters in hourly basis (Table 3) consistently show similar results for stations located in urban areas, suburban and rural areas. The correlation coefficient at all urban stations reached a maximum of 0.60 with values per station ranging from 0.35 to 0.75. Most of stations display values of MNGE and MNBE lying within the acceptable range defined by the US-EPA (Fig. 6c and d, respectively) with low values for MFB and MFE metrics. Table 3 and Fig. 6a also display the statistics for O_3 daily peaks. Rural areas are characterized by a general underestimation of O_3 daily peaks (~7 μg m^{-3}) while peak concentrations at urban stations are rather overestimated (8.4 μg m^{-3}) (Fig. 6b). High correlations are noted for each type of station. In summary the modeling system used in this study performs well with respect to the simulation of high O_3 concentrations over Spain. However, an overestimation of nocturnal values is depicted with recurrent low daily variations due to uncertainties in the modeled nocturnal NO_x cycle, which is a common feature in chemical transport models.

Stations influenced by traffic emissions (i.e., high-NO_x environments) are correctly characterized with a pronounced daily O_3 variability due to the O_3 destruction leaded by high NO_x. To complement such finding, Fig. 7, representing the O_3 model-to-observation bias as a function of the modeled NO_2 concentrations for all the 68 stations measuring both NO_2 and O_3, is proposed in order to evaluate the performances of the model with respect to the NO_x/O_3 chemistry.

While a deviation from the O_3 bias is mainly constrained by the lateral chemical boundary conditions, the width of the plotted dataset is controlled by the chemical mechanism implemented in the model. This figure clearly shows that the highest uncertainties in the reproduction of O_3 levels are related to NO_2-limited regime. Under this regime, corresponding to background conditions, the O_3 bias is slightly shifted to the right, meaning that the modeled O_3 tends to overestimate observed values, specifically during nighttime (also see mean observed and modeled values for rural stations in Table 3). As a contrary, the width of O_3 model-to-observation biases decreases with increasing modeled NO_2. Such behavior reflects the better representation of the NO_x/O_3 chemistry under non-limited-NO_2 regimes, but it also shows that the chemistry under higher NO_2 regime has a reduced dependency to the lateral chemical conditions of the model (no shift on the *X*-axis). As an example, data from Víznar (Rural Background, light grey triangles) and Recoletos (Urban Traffic, dark grey squares) are overlaid on the figure. The O_3 bias at Víznar displays a wide variability related to low modeled NO_2 whereas the bias for Recoletos markedly diminishes with increasing modeled NO_2. Such description confirms high sensitivity of the model to NO_2 regimes. This behavior highlights the need to better characterize the emission inventory in either rural (see discussion in Section 3.1) or urban areas. The curve interpolating the average O_3 bias in vertical also confirms the higher bias values under low NO_2 regime (maximum bias O_3 ~22 μg m^{-3} for $[NO_2]_{model} = 15$ μg m^{-3}), while it remains significantly lower for NO_2 modeled concentration above 60 μg m^{-3}.

Fig. 8 shows the temporal series of the Recoletos (UT) and Víznar (RB) stations for O_3 and NO_2. There is a high correlation between O_3 and NO_2 in the two different environments.

The annual mean distribution of O_3 over the IP is shown in Fig. 4b. Highest mean concentrations are located in the open Mediterranean Sea (up to 90 μg m^{-3}) and the Spanish Mediterranean coast (~80 μg m^{-3}). Such concentrations are favored by the prevailing intense photochemistry in the region (EEA, 2005; Vautard et al., 2005b), the local formation and transport (Lelieveld et al., 2002; Gerasopoulos et al., 2005; Cristofanelli and Bonasoni, 2009), the persistent subsidence over the region (Millán, 2002) and the low O_3 dry deposition over sea. The Spanish oceanic region in the north and north-western Spain, characterized by high frequency of precipitation presents lower O_3 levels than the Spanish arid and Mediterranean regions. The wet deposition of O_3 is an important sink in the oceanic

Table 3
Annual statistics for O_3 (hourly and daily peaks) obtained with CALIOPE over Spain for 2004 at the RedESP stations in hourly basis. Statistics are calculated according to four categories: over all stations ("All"), rural stations ("Rural"), suburban stations ("Suburban") and urban stations ("Urban"). Stations/data points column indicates the number of stations (values before slash) and the number of pair measurement-model (values after slash), respectively, used to compute the statistics. The calculated statistics are measured mean ($\mu g\ m^{-3}$), modeled mean ($\mu g\ m^{-3}$), correlation coefficient (r), root mean square error (RMSE, $\mu g\ m^{-3}$), mean fractional bias (MFB, %) and error (MFE; %), mean normalized bias error (MNBE, %) and gross error (MNGE; %). All metrics, except for measured mean, modeled mean and r, are calculated with an 80 $\mu g\ m^{-3}$ cut-off value (see US-EPA, 1991; Russell and Dennis, 2000).

Pollutant	Category	Stations/data points	Measured mean	Modeled mean	r	RMSE	MFB	MFE	MNBE	MNGE
O_3 hourly	All	82/673,608	57.4	71.0	0.57	24.1	−9.3	21.2	−6.0	19.2
	Rural	33/272,923	70.1	76.2	0.51	24.1	−11.2	21.8	−7.7	19.5
	Suburban	25/204,225	51.7	67.5	0.56	24.7	−8.7	20.7	−5.4	18.9
	Urban	24/196,460	45.4	67.4	0.60	23.4	−4.2	19.8	−1.2	18.9
O_3 peaks	All	82/673,608	86.1	85.5	0.64	25.9	−9.8	21.2	−6.6	19.5
	Rural	33/272,923	93.8	86.9	0.67	24.8	−12.9	21.3	−9.7	19.0
	Suburban	25/204,225	84.7	84.1	0.65	27.9	−9.0	21.5	−5.7	19.9
	Urban	24/196,460	76.6	85.0	0.63	25.8	−4.2	20.7	−1.0	20.0

regions, meanwhile local generation and transport are the processes which contribute to O_3 levels in arid and Mediterranean regions.

Fig. 4b also highlights significant levels over the major Spanish mountain ranges such as the Pyrenean chain, the Baetic Cordillera (southeastern Spain) or the Sierra Norte (laying north of Madrid in a west-to-northeast direction), reflecting the O_3 vertical gradient in the atmosphere.

O_3 is found lowest (~50 $\mu g\ m^{-3}$) in either regions of low precursor emissions (northern and southern plateaus) or in areas affected by large NO-to-NO_2 concentration ratios (e.g., zones of intense on-road and ship traffic). Reactions involving nitrogen oxides are well-known key reactions controlling the amount of O_3 in the troposphere (Fishman and Crutzen, 1978). In this chemical regime reactions between NO_2 and O_3 prevail, leading to low levels of O_3. These areas comprise the major Spanish metropolitan cities (i.e., Madrid, Barcelona, Valencia, Sevilla), highways of high traffic flow (like NO_2, see Section 3.1) and the major shipping routes in the Mediterranean Sea.

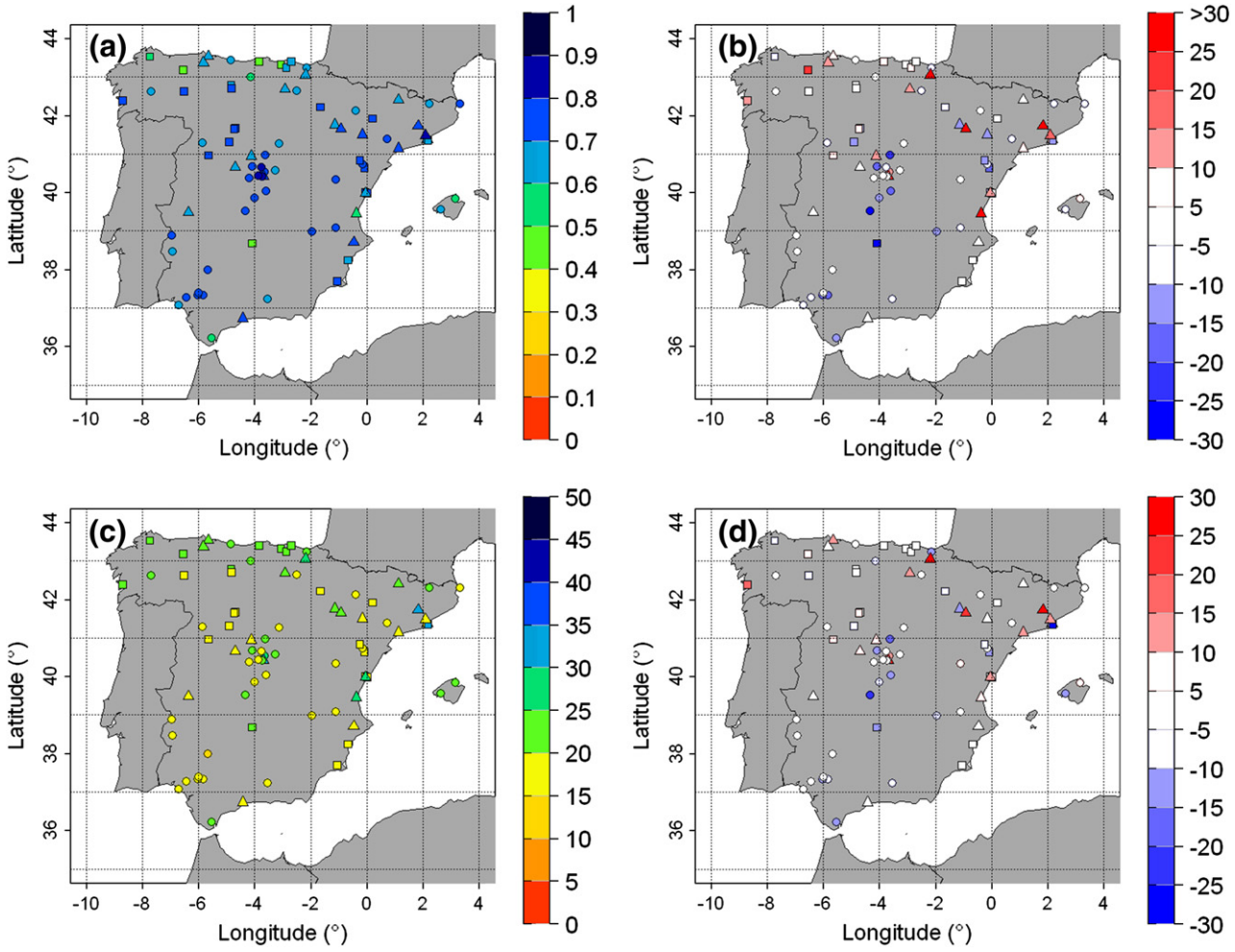

Fig. 6. Spatial distribution of the statistics for O_3 over 2004 at the RedESP stations: daily peak correlation coefficient (r) (a), annual mean bias (MB, in $\mu g\ m^{-3}$) for daily peak (b), mean normalized gross error (MNGE, in %) in hourly basis (c), and mean normalized bias error (MNBE, in %) in hourly basis (d). Note that MB, MNGE and MNBE are calculated with 80 $\mu g\ m^{-3}$ cut-off according to US-EPA (1991) and Russell and Dennis (2000). The various symbols represent the major emission types affecting each station (see Fig. 2).

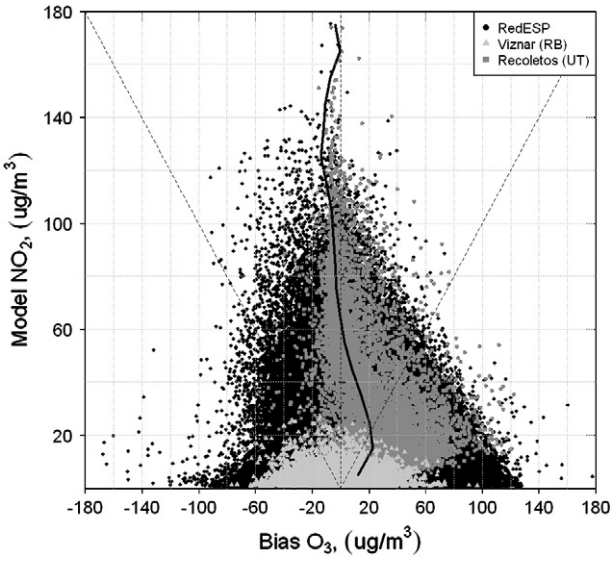

Fig. 7. Modeled NO_2 levels versus model-observation O_3 bias. The 68 stations measuring both NO_2 and O_3 are represented on an hourly basis (black dots). Data from Viznar, a rural background station (light grey triangles) and Recoletos, urban traffic (dark grey squares) are also displayed. The vertical black curve represents the average concentration on the *X*-axis every 10 μg m^{-3} from the vertical axis.

3.3. Sulfur Dioxide

From a total of 45 stations measuring SO_2, 13 are located in urban areas, 14 are in suburban and 18 are in rural areas, respectively. In Spain, SO_2 is mainly produced by power generating and transformation industries. Indeed, Linares and Romero (2000) reported that electricity generation contributes 66% to the total SO_2 emitted in Spain. These very localized industries generate large plumes of high-SO_2 content affecting the air quality on a local to national scale. Modeling SO_2 for air quality purposes is a complex issue, since the accuracy in the meteorological patterns is crucial for the determination of plume dynamics. Also, the variability on the sub-grid scale must be considered when comparing model results with measured data.

The hourly SO_2 variability and levels, averaged over all available stations, are very well captured by the modeling system (Fig. 3b). Episodic extreme values are underestimated in general, although the model is capable of reproducing the trend. Annual MB are low, from −3.1 for urban to 0.6 μg m^{-3} for suburban stations (Table 2). Due to the frequently episodic character of high SO_2 events and their dependency to meteorology correlation coefficients are rather low ($r = 0.14$ for urban/suburban stations; 0.28 for rural stations). Highest correlations were obtained for background stations ($r = 0.34$). MFB values show good performance comparing with the other primary pollutants (−47.1%<MFB <−23.8%) but MFE values highlight the need to further improve the modeled SO_2 physico-chemistry. Among the 45 stations measuring SO_2 in the Peninsula, the model-to-data comparison was distinctly unsatisfactory for three locations (7% of the total). Two of these locations were found in the same grid cell as large power plants (Abanto and Grao). A third station ("Salamanca2" in the city of Salamanca) displays high SO_2 measured concentrations which are strongly underestimated by the model. Such behavior may be explained by emission sources unaccounted by the model system or by the erroneous coordinates of the instrument.

In Spain, Baldasano et al. (2008a) reported that combustion in energy and transformation industries contributes 83% to the total SO_2 emitted in Spain. In this framework, the SO_2 is emitted mainly from large isolated point sources, instantaneously mixed into high layers in the atmosphere and transported and dispersed following the plume dynamic. The mean chemical distribution of SO_2 over the IP, shown in Fig. 4c, is characterized by two major patterns. First, the Spanish territory is marked by various emission hot-spots often reaching air concentrations above 15 μg m^{-3}. These localized sources originate mainly from power plants and refineries.

Northern Spain suffers substantial SO_2 mean annual levels of up to ~10 μg m^{-3} due to the presence of geographically close power plants and refineries in the area of Galicia, Ponferrada, Asturias and Bilbao. SO_2 reaches maximum levels (~50 μg m^{-3}) near the two refineries in Bilbao and La Coruña. The SO_2 dispersion pattern in north-western Spain is significantly dominated by the northern and north-western winds that transport SO_2 inland. Eastern Spain is mostly affected by a thermo-electrical power plant from Teruel (Aragón region), the pattern is dominated by the canalization of the Ebro valley towards the Mediterranean sea. The southern Spanish plateau displays high SO_2 levels around Puertollano (Castilla-La Mancha region) due to the presence of a refinery and two power plants.

In the urban areas the SO_2 dispersive pattern remains ~6 μg m^{-3}; in Madrid and Barcelona cities the levels of SO_2 are the sum of two contributions, the on-road traffic and the cogeneration plants. Minimum concentrations from unpolluted areas display mean values near 0.5–2 μg m^{-3}.

The second pattern dissociated from this figure is the shipping route from the Atlantic, through the Strait of Gibraltar, toward the major Mediterranean harbors. Ship emissions are large contributors to the total SO_x concentrations along the main ship tracks due to fuel combustion of high sulfur content (Corbett and Fischbeck, 1997; Corbett and Koehler, 2003), although ship emission abatement strategies are under current application (Internacional Maritime Organization and Marine Environment Protection Committee, 2001). These emissions from maritime zones lead to coastal mean SO_2 concentrations from 2 to 8 μg m^{-3} on annual average, with a maximum of 12–18 μg m^{-3} in the narrow Gibraltar regions with a dispersion pattern dominated by western winds. The SO_2 contribution of shipping route in this area is combined with the contribution from one large refinery, industrial processes, and electric generation carried out in the Gibraltar bay.

3.4. Particulate Matter

A total of 44 RedESP stations measured particulate matter concentrations over the IP and the Balearic Islands for the year 2004. 12 Stations were located in rural areas, 17 are in suburban and 15 are in urban areas, respectively. Among these 44 stations, the model represented the PM concentrations fairly well at 17 locations (nearly 40% of the total). These locations were mostly background rural. In these areas mean concentrations are often low with episodic high concentration peaks. The implementation of the Sahara desert dust contribution from the BSC-DREAM8b model is responsible for the satisfactory representation of such concentration peaks. The evaluation of the modeling system highlighted less accurate modeled levels at suburban and urban locations mostly influenced by background emissions. Model-to-data comparisons in urbanized areas of industrial or traffic emissions showed lowest accuracy. We attribute such behavior to the inadequate characterization of emission sources in areas of intense human activity.

Fig. 3c clearly highlights two distinct aspects of the model in the representation of hourly averaged PM10 concentrations at all available stations. Modeled concentrations were persistently underestimated throughout the year 2004. This underestimation is a common feature of most of the current regional models (Pay et al., 2010a). The annual MB amounts to −21.8 μg m^{-3} with an annual RMSE value of 33.4 μg m^{-3} (Table 2). On the other hand, the general PM10 dynamics are well captured, with the major events correctly modeled and synchronized with measured amounts. The mean correlation for all stations amounts to 0.38 with higher correlations

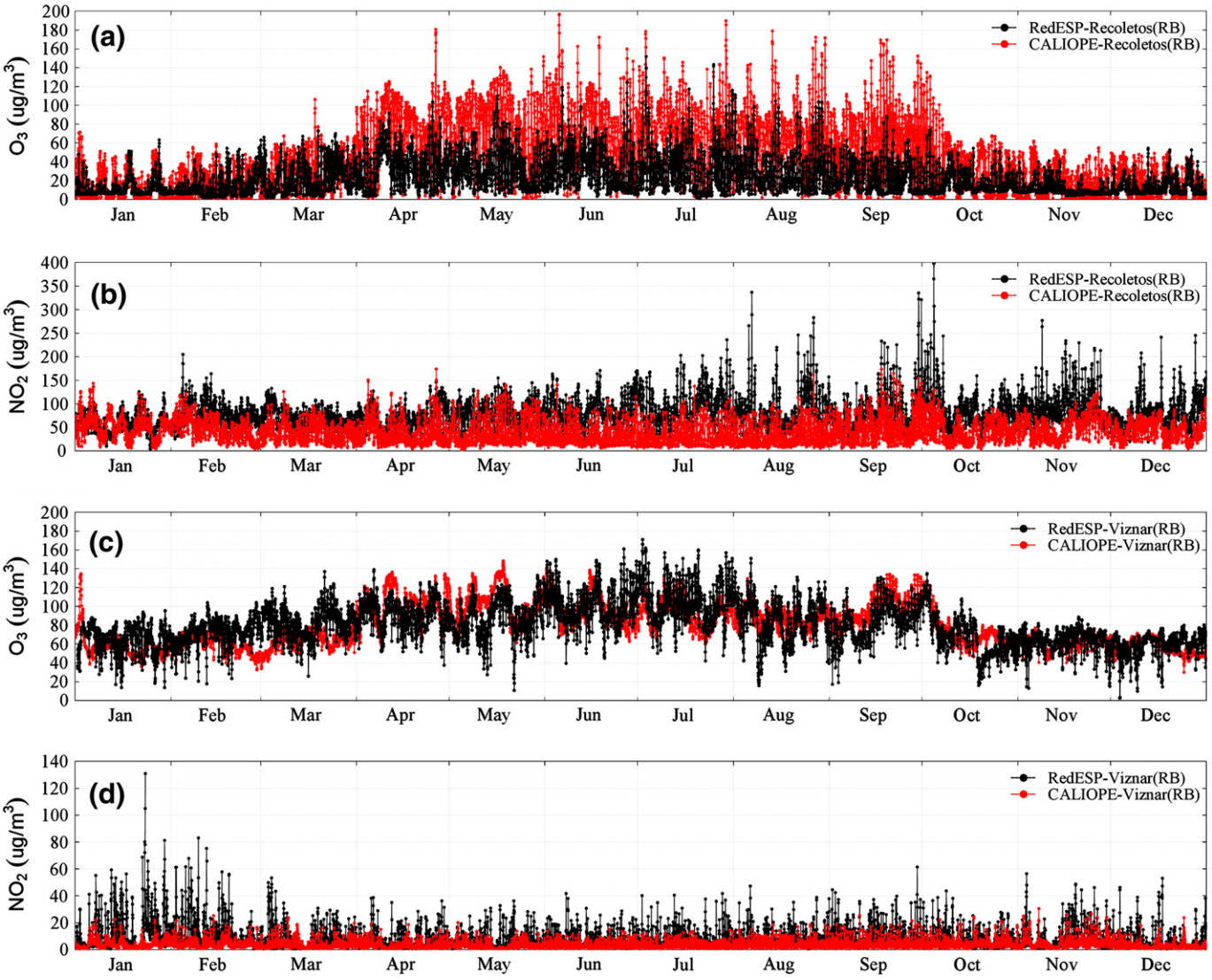

Fig. 8. Modeled (marked red lines) and measured (marked black lines) time series of hourly mean concentrations (in $\mu g\ m^{-3}$) for O_3 and NO_2 at the urban traffic station (UT) of Recoletos (a and b, respectively) and at the rural background (RB) station of Víznar (c and d, respectively) over the year 2004.

at rural stations ($r = 0.43$, ranging from 0.28 to 0.58 per station). Due to the important underestimation of the model concentrations, MFB and MFE values are undoubtedly ranging above the criteria for acceptable model performances proposed by Boylan and Russell (2006).

Fig. 4d shows the annual average pattern of natural and anthropogenic PM10 over the IP for 2004. Concentrations show a large variability across Spain depending on emission sources, climate and reactivity/stability of particulate species (see Querol et al., 2001, 2003, 2004a, 2008; Rodríguez et al., 2002; Viana et al., 2005). The modeled spatial distribution of annual PM10 levels shows that particle concentrations reach high values (~15 $\mu g\ m^{-3}$) in large cities like Madrid, Barcelona, Valencia, and Bilbao. There is an important contribution of exhaust and non-exhaust emissions from road transport in urban areas.

Marine aerosols contribute nearly 3 and 5 $\mu g\ m^{-3}$ to the annual mean PM10 concentration over the Mediterranean and Atlantic coasts, respectively (not shown). This difference in concentration reflects the higher wind speeds and fetch distances in the Atlantic than in the Mediterranean basin leading to more transport of sea salt aerosols from the Atlantic open ocean to the coasts. The contribution of marine aerosols to PM10 annual concentrations over the open ocean ranges from 6 (Mediterranean basin) to 9 $\mu g\ m^{-3}$ (Atlantic) which is consistent with model data from Manders et al. (2010).

In the north, the industrial areas in Castellón dominated by ceramic industry, present high levels of PM10, dispersed along a perpendicular axis to the coast. Mediterranean coast shows PM10 dispersion pattern influenced by sea-breezes combined with upslope winds to create recirculations along the coast and within the western Mediterranean basin. In summer the higher temperatures and solar radiation lead to the formation of secondary aerosols contributing to the levels of particulate matter. The Ebro valley acts by channelling particulate matter flow inland. Meanwhile in the northern coastal Spain the Atlantic winds dominate the transport of particulate matter inland.

Large sources of SO_2 located in wet Spain region, in the north, (Fig. 4c) do not contribute efficiently to the secondary inorganic aerosol since high dispersion and removal by wet deposition are important processes in this region (not shown). In the southern part of Spain, African dust outbreaks contribute significantly to the aerosol loadings, ranging from to 10 to 20 $\mu g\ m^{-3}$. The largest annual mean contribution of desert dust coincides with the Sierra Nevada mountain range with values reaching up to 30 $\mu g\ m^{-3}$. Such concentrations are the consequences of (1) the mountain range location within the main

zone of dust deposition (70% of dust export is deposited within the first 2000 km, Jaenicke and Schütz, 1978) and (2) the existence of several peaks within the mountain range 3000 m above sea level (asl) which corresponds to the altitude range for Saharan dust transport (between 1500 and 4000 m asl, Talbot et al., 1986; Olmo et al., 2008).

4. Exceedances of Ozone During Summertime

This section analyzes the O_3 exceedances during the high O_3 season (from April to September) when O_3 concentrations present peaks which frequently exceeded 120 μg m^{-3}, reaching 200 μg m^{-3}. The target value set in the European regulation is 120 μg m^{-3}, not to be exceeded on more than 25 days per calendar year averaged over 3 years (averaging as the maximum daily 8-h mean, European Commission, 2008). Fig. 9 shows the number of days exceeding the concentration value of 120 μg m^{-3} for the 8-h maximum O_3 concentration and the VOC/NO_x mass ratio over the land domain (Fig. 9a) and over the entire domain, including the ocean (Fig. 9b). The VOC/NO_x ratio is calculated as hourly average and is represented in logarithmic scale, since the ratio ranges from 1 to 10^6.

There is an overlap among ratios and number of days with exceedances. The number of exceedances is higher than 45 days where log(VOC/NO_x) ratio is between 3 and 4.5, approximately. Such situation corresponds to zones downwind of main NO_x emission sources (see annual mean concentration of NO_2 in Fig. 4a) from the two largest Spanish cities (Madrid and Barcelona, see locations in Fig. 9) and industrial areas along the eastern Spanish Mediterranean coast (Tarragona, Valencia and Castellón; see locations in Fig. 9). Dynamics of pollutant during summer and primary emission sources along the eastern coast and the central plateau of the IP determinate the location of the calculated exceedances. Several studies performed over the western Mediterranean basin (e.g., Gangoiti et al., 2001; Jiménez and Baldasano, 2004; Stein et al., 2005; Jiménez et al., 2006; Jiménez-Guerrero et al., 2008b; Gonçalves et al., 2009) are in agreement with our findings. Along the coast the sea-breezes and mountain-valley winds contribute to the accumulation and recirculation of aged air masses and O_3 aloft. Besides, over the central plateau flows are dominated by the development of the IP Thermal Low (ITL). Several deep convective cells coupled with the ITL inject aged pollutant for the Madrid area and those transported previously from coastal area. On the other hand, the number of exceedances is less than 30 days for log(VOC/NO_x) ratio higher than 4.75, that regime, represented in white color in Fig. 9, covers the northern and southern Spanish plateaus, where there is no high density of anthropogenic emissions. Note that a quarter of the IP presents more than 30 days exceeding the value of 120 μg m^{-3} for the 8-h maximum O_3 concentration.

In general, there is a significant anti-correlation ($r=-0.71$) between O_3 exceedances and the log(VOC/NO_x) ratio for the entire domain when only the inland O_3 formation is considered (Fig. 9a). For high ratios, there is a NO_x limitation regime, and no O_3 exceedances are detected once there is not enough NO_x available. However, when we calculate the aforementioned correlation over the entire domain, including the ocean (Fig. 9b), the anti-correlation slightly decreases ($r=-0.63$) as a result of two different behaviors. First, the Strait of Gibraltar region presents the lowest log(VOC/NO_x) ratio (equal to 3) and no exceedances are detected (see Section 3.2). The frequent shipping traffic and the high density of industry in the area generate important NO_x emissions, VOC concentrations are not high enough to produce O_3; moreover the O_3 loss is high due to NO_x emissions act as O_3 sinks (Marmer et al., 2009). The opposite happens over the western Mediterranean basin which shows the highest log(VOC/NO_x) ratio (over 5) and many exceeding days (more than 45). As we mentioned before, the complex layout of the coasts and surrounding mountain favors that the Mediterranean Sea acts as a reservoir of aged pollutants. Furthermore in summer the meteorological condition (high pressure, stability, clear sky and high solar radiation intensity) enhances photochemical processes and emissions of biogenic volatile organic compounds to the atmosphere (NO_x limited regime). Not only O_3 formation due to local and regional sources but also long-range transport of European air toward the Mediterranean basin (Lelieveld et al., 2002) could be important causes of the O_3 exceedances of the limit value. Furthermore, dry deposition over open ocean remains near zero (not shown here). All together contribute to increase levels of O_3 (lifetime typically of few weeks in summer, Seinfeld and Pandis, 1998).

5. Summary and Conclusions

This work presents the evaluation and the assessment of the CALIOPE air quality forecasting system (namely WRF-ARW/HERMES/CMAQ/BSC-DREAM8b) for a full-year simulation for 2004 over Spain. CALIOPE was applied with high resolution (4 km × 4 km, 1 h) using the HERMES emission model specifically developed for Spain. The evaluation of the modeling results for gas-phase pollutants (O_3, NO_2 and

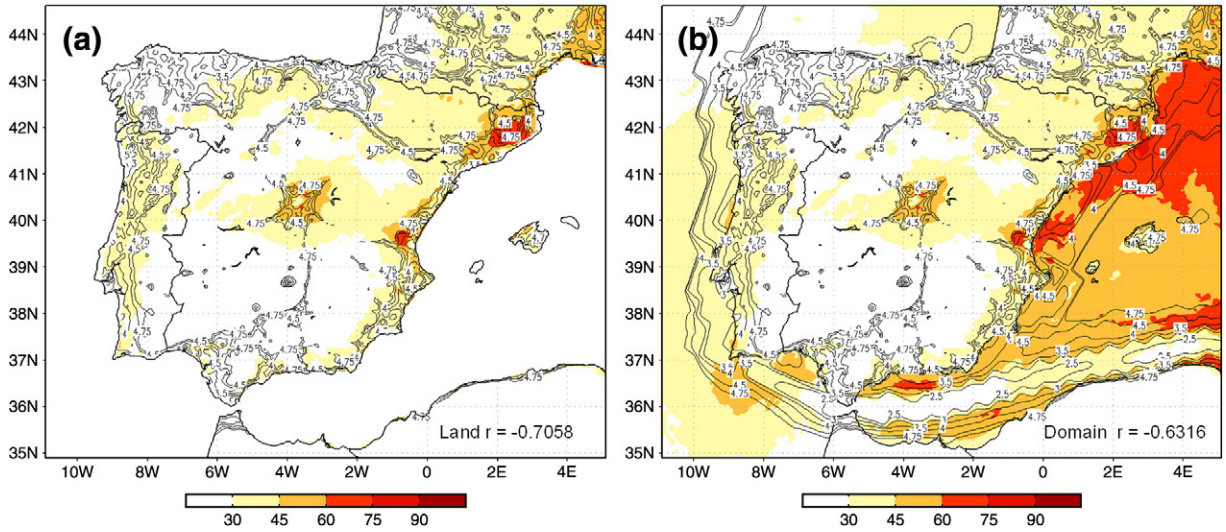

Fig. 9. Days exceeding the concentration value of 120 μg m^{-3} for the 8-h maximum O_3 concentration (color scale) and the logarithm of the VOC/NO_x concentration ratio (contour lines) during the high O_3 season (from April to September) in 2004 simulated by CALIOPE at a 4 km × 4 km over the land domain (a) and the entire domain (b). In both cases, correlation between days exceeding the concentration value of 120 μg m^{-3} and the logarithm of the VOC/NO_x concentration ratio is showed at the bottom-right.

SO_2) and particulate matter (PM10) on an hourly basis showed a strong dependency of the performance of the model on the type of environment (urban, suburban and rural) and the dominant emission sources (traffic, industrial, and background). For NO_2, the best model behavior corresponds to both background rural stations and urban stations located in very large cities such as Madrid or Barcelona. With respect to O_3, stations influenced by traffic emissions (NO_x-dominated) are better characterized with a more pronounced daily variability. NO_x/O_3 chemistry is better represented under non-limited-NO_2 regimes. For each station category, annual O_3 (hourly and peaks) statistics meet the range defined by the US-EPA and European regulation for an acceptable performance of the model. Results show that a quarter of the Iberian Peninsula is affected by more than 30 days exceeding the value of 120 $\mu g\ m^{-3}$ for the 8-h maximum O_3 concentration.

The general spatial patterns and temporal characteristics simulated by CALIOPE for gas-phase pollutants and particulate matter are consistent with other studies and surveys. SO_2 is mainly produced from isolated point sources (power generation and transformation industries) which generate large plumes of high SO_2 concentration affecting the air quality on a local to national scale where the meteorological pattern is crucial, whereas NO_2 concentration at ground level is dominated mainly by traffic emissions, which are subjected to a much stronger temporal variation than the SO_2 emissions.

PM10 and NO_2 mean levels are persistently underestimated. Highest PM10 mean bias corresponds to suburban and urban location mostly influenced by background emission. On the other hand, highest NO_2 errors are found in urban stations which are likely influenced by high local emission sources from urban activities. Such behavior is attributed to the incomplete characterization of emissions from small cities and to the influence of the model resolution on sub-grid emission sources.

Despite the accurate performance of the modeling system, several aspects are now under further research in the framework of the CALIOPE project. Wind-blown dust should be taken into account since such source contributes to the underestimation of the total concentration of PM10, especially in dry and arid regions such Spain. Biomass burning and natural NO_x are currently not treated in the CALIOPE modeling system and could contribute to the NO_2 underestimation. In addition, ammonia emission and particulate matter from vegetated and agricultural areas in HERMES are under a continuous improvement. Last, a new version of CMAQ is being implemented in the MareNostrum supercomputing (CMAQv4.7) featuring a new aerosol module, AERO5, which contains substantial scientific improvements over the AERO4 released in version 4.5, especially devoted to improve secondary organic aerosol formation and dynamic interactions of fine and coarse aerosol.

The present analysis demonstrates that the high spatial resolution (4 km×4 km) applied in the CALIOPE forecasting system correctly address the air pollution behavior in (1) urban/industrial areas with a pervasive influence of anthropogenic emissions on a local scale and (2) areas with very complex terrains and meteorology like southern Europe. Therefore, the system has been implemented and evaluated operationally and air quality forecasts can be found in http://www.bsc.es/caliope.

Acknowledgments

The authors wish to thank the CEAM, CIEMAT and CSIC-IJA centers for their collaboration in the project. Also, thanks to S. Basart and C. Pérez for providing the BSC-DREAM8b outputs. M. Piot and L. González are also thanked. for their work related to the CALIOPE system. This work is funded by the CALIOPE project of the Spanish Ministry of the Environment (441/2006/3-12.1, A357/2007/2-12.1, 157/PC08/3-12.0). The Spanish Ministry of Science and Innovation is also thanked for the Formación de Personal Investigador (FPI) doctoral fellowship held by María Teresa Pay (CGL2006-08903). All simulations were performed on the MareNostrum supercomputer hosted by the Barcelona Supercomputing Center.

Appendix A. Supplementary data

Supplementary data to this article can be found online at doi:10.1016/j.scitotenv.2011.01.041.

References

Amann M, Bertok I, Cofala J, Gyarfas F, Heyes C, Klimont Z, et al. Baseline Scenarios for the Clean Air for Europe (CAFE) programme. Technical Report. European Commission, DG Environment, Dir. C Environment and Health; 2004.

Amato F, Pandolfi M, Escrig A, Querol X, Alastuey A, Pey J, et al. Quantifying road dust resuspension in urban environment by multilinear engine: a comparison with pmf2. Atmos Environ 2009a;43:2770–80.

Amato F, Pandolfi M, Viana M, Querol X, Alastuey A, Moreno T. Spatial and chemical patterns of PM10 in road dust deposited in urban environment. Atmos Environ 2009b;43:1650–9.

Amato F, Nava S, Lucarelli F, Querol X, Alastuey A, Baldasano JM, et al. A comprehensive assessment of PM emissions from paved roads: real-world emission factors and intense street cleaning trials. Sci Total Environ 2010;408:4309–18.

Appel KW, Gilliland A, Sarwar G, Gilliam RC. Evaluation of the community multiscale air quality (CMAQ) model version 4.5: uncertainties and sensitivities impacting model performance: part I e ozone. Atmos Environ 2007;41(40):9603–13.

Appel KW, Bhave PV, Gilliland AB, Sarwar G, Roselle SJ. Evaluation of the community multiscale air quality (CMAQ) model version 4.5: sensitivities impacting model performance; part II e particulate matter. Atmos Environ 2008;42(24):6057–66. doi:10.1016/j.atmosenv.2008.03.036.

Arévalo G, Salvador R, Gassó S, Millán M, Baldasano JM. Application of a high-resolution emission model in Valencia Community (Spain). Air Pollution 2004. Rhodes, Greece: WIT Press; 2004. p. 31–40.

Baldasano JM, Cremades L, Soriano C. Circulation of air pollutants over the Barcelona geographical area in summer. Proceedings of Sixth European Symposium Physic-Chemical Behavior of Atmospheric Pollutants. Varese (Italy), 18–22 October, 1993. Report EUR 15609/EN: 474–479; 1994.

Baldasano JM, Jiménez-Guerrero P, Jorba O, Pérez C, López E, Güereca P, et al. Caliope: an operational air quality forecasting system for the Iberian Peninsula, Balearic Islands and Canary Islands—first annual evaluation and ongoing developments. Adv Sci Res 2008a;2:89–98.

Baldasano JM, Güereca LP, López E, Gassó S, Jiménez-Guerrero P. Development of a high-resolution (1 km×1 km, 1 h) emission model for Spain: the High-Elective Resolution Modelling Emission System (HERMES). Atmos Environ 2008b;42:7215–33.

Binkowski FS. Aerosols in models-3 cmaq. In: Byun DW, Ching JKS, editors. Science Algorithms of the EPA Models-3 Community Multiscale Air Quality (CMAQ) Modeling System. EPA; 1999. p. 10–23.

Binkowski FS, Roselle SJ. Models-3 community multiscale air quality (cmaq) model aerosol component. 1. Model description. J Geophys Res 2003;108(D6):4183. doi:10.1029/2001JD001409.

Binkowski FS, Shankar U. The regional particulate model 1. Model description and preliminary results. J Geophys Res 1995;100(D12):26191–209.

Boylan J, Russell A. Pm and light extinction model performance metrics, goals, and criteria for three-dimensional air quality models. Atmos Environ 2006;40:4946–59.

Brunekreef B, Holgate ST. Air pollution and health. Lancet 2002;360(9341):1233–42. doi:10.1016/S0140-6736(02)11274-8.

Byun DW, Ching JKS. Science algorithms of the EPA Models-3 Community Multiscale Air Quality (CMAQ) modeling system. National Exposure Research Laboratory, US Environmental Protection Agency, Research Triangle Park, NC: Atmospheric Modeling Division; 1999. 27711.

Byun D, Schere KL. Review of the governing equations, computacional algorithms, and other components of the Models-3 Community Multiscale Air Quality (CMAQ) modeling system. Appl Mech Rev 2006;59(2):51–77.

Carter WPL. Implementation of the SAPRC-99 Chemical Mechanism into the Models-3 Framework. Report to the United States Environmental Protection Agency, January 29; 2000. Available at http://www.cert.ucr.edu/~carter/absts.htm#s99mod3.

Chang JC, Hanna SR. Air quality model performance evaluation. Meteorol Atmos Phys 2004;87:167–96.

Ching J, Herwehe J, Swall J. On joint deterministic grid modeling and sub-grid variability conceptual framework for model evaluation. Atmos Environ 2006;40:4935–45.

Corbett JJ, Fischbeck P. Emissions from ships. Science 1997;278(5339):823–4. doi:10.1126/science.278.5339.823.

Corbett JJ, Koehler HW. Updated emissions from ocean shipping. J Geophys Res 2003;108(D20):4650. doi:10.1029/2003JD003751.

Cox WM, Tikvart JA. Statistical procedure for determining the best performing air quality simulation model. Atmos Environ 1990;24:2387–95.

Cristofanelli P, Bonasoni P. Background ozone in the southern Europe and Mediterranean area: influence of the transport processes. Environ Pollut 2009;157:1399–406.

Cuvelier C, Thunis P, Vautard R, Amann M, Bessagnet B, Bedogni M, et al. Citydelta: a model intercomparison study to explore the impact of reductions in European cities in 2010. Atmos Environ 2007;41:189–207.

de Leeuw F, Vixseboxse E. Reporting on ambient air quality assessment—preliminary results for 2008. Technical ReportThe European Topic Centre on Air and Climate Change (ETC/ACC) Technical Paper 2009/10; 2010.

Denby B, Larssen S, Guerreiro C, Li L, Douros J, Moussiopoulos N, et al. Guidance on the use of models for the European Air Quality Directive. A working document of the Forum for Air Quality Modelling in Europe FAIRMODE. In: Denby B, editor. Technical Report Version 4.2ETC/ACC report; 2010.

EEA. Air pollution by ozone in Europe in summer 2004. Technical Report. 3/2005, Copenhagen, Denmark; 2005. http://reports.eea.eu.int.
EEA. Air pollution by ozone across Europe during summer 2008. Technical Report. 2/2009, Copenhagen, Denmark; 2009a. http://reports.eea.eu.int.
EEA. Spatial assessment of PM10 and ozone concentrations in Europe (2005). Technical Report. 1/2009, Copenhagen, Denmark; 2009b. http://reports.eea.eu.int.
EEA. Air pollution by ozone across Europe during summer 2009. Technical Report. 2/2010, Copenhagen, Denmark; 2010. http://reports.eea.eu.int.
European Commission. Forest fires in Europe 2004. Report 5. Official Publication of the European Commission; 2005. http://www.fire.uni-freiburg.de/programmes/eu-comission/EU-Forest-Fires-in-Europe-2004.pdf. S.P.I.05.147 EN., Source.
European Commission. Directive 2008/50/EC of the European Parliament and of the Council of 21 May 2008 on ambient air quality and cleaner air for Europe. Technical Report 2008/50/EC, L152Off. J. Eur. Comm; 2008.
Fishman J, Crutzen P. The origin of ozone in the troposphere. Nature 1978;274:855–8.
Folberth G, Hauglustaine DA, Lathière J, Brocheton J. Interactive chemistry in the laboratoire de météorologie dynamique general circulation model: model description and impact analysis of biogenic hydrocarbons on tropospheric chemistry. Atmos Chem Phys 2006;6:2273–319.
Gangoiti G, Millán M, Salvador R, Mnatilla E. Long-range transport and re-circulation of pollutants in the western Mediterranean during the project regional cycles of air pollution in the west-central Mediterranean area. Atmos Environ 2001;35:6267–76.
Garber W, Colosio J, Grittner S, Larssen S, Rasse D, Schneider J, et al. Guidance on the Annexes to Decision 97/101/EC on Exchange of Information as revised by Decision 2001/752/EC. Technical Report. European Commission, DG Environment; 2002.
Gerasopoulos E, Kouvarakis G, Vrekoussis M, Kanakidou M, Mihalopoulos N. Ozone variability in the marine boundary layer of the eastern Mediterranean based on 7-year observations. J Geophys Res 2005;110:D15309.
Gery MW, Whitten GZ, Killus JP, Dodge MC. A photochemical kinetics mechanism for urban and regional scale computer modeling. J Geophys Res 1989;94(D10):12925–56.
Gonçalves M, Jiménez-Guerrero P, Baldasano J. Contribution of atmospheric processes affecting the dynamics of air pollution in south-western Europe during a typical summertime photochemical episode. Atmos Chem Phys 2009;9:849–64.
Gong SL. A parameterization of sea-salt aerosol source function for sub- and super-micron particles. J Geophys Res 2003;17:1097. doi:10.1029/2003GB002079.
Gryparis A, Forsberg B, Katsouyanni K, Analitis A, Touloumi G, Schwartz J, et al. Acute effects of ozone on mortality from the air pollution and health: a European approach project. Am J Respir Crit Care Med 2004;170(10):1080–7.
Guenther AB, Hewitt CN, Erickson D, Fall R, Geron C, Graedel T, et al. A global model of natural volatile organic compound emissions. J Geophys Res 1995;100:8873–92.
Hauglustaine DA, Hourdin F, Jourdain L, Filiberti MA, Walters S, Lamarque JF, et al. Interactive chemistry in the laboratoire de meteorologie dynamique general circulation model: description and background tropospheric chemistry evaluation. J Geophys Res 2004;D4(D04314). doi:10.1029/2003JD003,957.
Internacional Maritime Organization and Marine Environment Protection Committee. Prevention of air pollution from ships—sulfur monitoring 2000. Technical Report; 2001. London.
Jaenicke R, Schütz L. Comprehensive study of physical and chemical properties of the surface aerosols in the Cape Verde islands region. J Geophys Res 1978;83(C7):3585–99.
Janjic ZI. The step-mountain ETA coordinate model: Further developments of the convection, viscous sublayer and turbulence closure schemes. Mon Weather Rev 1994;122:927–45.
Jiménez P, Baldasano JM. Ozone response to precursor controls in very complex terrains: use of photochemical indicators to assess O_3-NO_x-VOC sensitivity in the northeastern Iberian Peninsula. J Geophys Res 2004;109:D20309. doi:10.1029/2004JD004985.
Jiménez P, Baldasano JM, Dabdub D. Comparison of photochemical mechanisms for air quality modelling. Atmos Environ 2003;37(30):4179–94. doi:10.1016/S1352-2310(03)00567-3.
Jiménez P, Lelieveld J, Baldasano JM. Multi-scale modeling of air pollutants dynamics in the northwestern Mediterranean basin during a typical summertime episode. J Geophys Res 2006;111(D18306):1-21. doi:10.1029/2005JD006516.
Jiménez-Guerrero P, Jorba O, Baldasano JM, Gassó S. The use of a modelling system as a tool for air quality management: annual high resolution simulations and evaluation. Sci Total Environ 2008a;390:323–40.
Jiménez-Guerrero P, Pérez C, Jorba O, Baldasano JM. Contribution of Saharan dust in an integrated air quality system and its on-line assessment. Geophys Res Lett 2008b;35(L03814). doi:10.1029/2007GL031580.
Kelly JT, Bhave PV, Nolte CG, Shankar U, Foley KM. Simulationg emission and chemical evolution of coarse sea-salt particles in the Community Multiscale Air Quality (CMAQ) model. Geosci Model Dev 2010;3:257–73.
Lam YF, Fu JS. A novel downscaling technique for the linkage of global and regional air quality modeling. Atmos Chem Phys 2009;9:9169–85.
Lelieveld J, Berresheim H, Borrmann S, Crutzen PJ, Dentener FJ, Fischer H, et al. Global air pollution crossroads over the Mediterranean. Science 2002;298:794–9.
Linares P, Romero C. A multiple criteria decision making approach for electricity planning in Spain: economic versus environmental objectives. J Oper Res Soc 2000;51(6):736–43.
Manders AMM, Schaap M, Querol X, Albert MFMA, Vercauteren J, Kuhlbusch TAJ, Hoogerbrugge R. Sea salt concentrations across the European continent. Atmos. Environ 2010;44:2434–42.
Marmer E, Dentener F, Aardenne J, Cavalli F, Vignati E, Velchev K, et al. What can we learn about ship emission inventories from measurements of air pollutants over the Mediterranean Sea? Atmos Chem Phys Discuss 2009;9:7155–211.
Menut L, Bessagnet B. Atmospheric composition forecasting in Europe. Ann Geophys 2010;28:61–74.
Michalakes J, Dudhia J, Gill D, Henderson T, Klemp J, Skamarock W, et al. The weather research and forecast model: software architecture and performance. In: Mozdzynski EG, editor. To appear in proceeding of the Eleventh ECMWF Workshop on the Use of High Performance Computing in Meteorology, 2529 October 2004, Reading, U.K.; 2004. p. 117–24.
Millán MM. Ozone dynamics in the Mediterranean basin, a collection of scientific papers resulting from the MECAPIP, RECAPMA and SECAP Projects. Technical Report. European Commission and CEAM; 2002.
Millán MM, Salvador R, Mantilla E. Photooxidant dynamics in the Mediterranean basin in summer: results from European research projects. J Geophys Res 1997;102(D7):8811–23.
Millán MM, Sanz MJ, Salvador R, Mantilla E. Atmospheric dynamics and ozone cycles related to nitrogen deposition in the western Mediterranean. Energy Policy 2002;118:167–86.
Nenes A, Pilinis C, Pandis SN. ISORROPIA: a new thermodynamic equilibrium model for multiphase multicomponent inorganic aerosols. Aquat Geochem 1998;4(1):123–52. doi:10.1023/A:1009604003981.
Nickovic S, Kallos G, Papadopoulos A, Kakaliagou O. A model for prediction of desert dust cycle in the atmosphere. J Geophys Res 2001;106(D16):18113–29. doi:10.1029/2000JD900794.
Olmo FJ, Quitantes A, Lara V, Lyamani H, Alados-Arboledas L. Aerosol optical properties assessed by an inversion method using the solar principal plane for non-spherical particles. J Quant Spectrosc Radiat Transfer 2008;109:1504–16.
Ortiz de Zárate I, Ezcurra A, Lacaux JP, Dinh PV, de Argandoña JD. Pollution by cereal waste burning in Spain. Atmos Res 2005;73(1–2):161–70. doi:10.1016/j.atmosres.2004.07.006.
Pandis SN, Harley RA, Cass GR, Seinfeld JH. Secondary organic aerosol formation and transport. Atmos Environ Part A 1992;26:2269–82.
Parra R, Gassó S, Baldasano JM. Estimating the biogenic emissions of non-methane volatile organic compounds from the North Western Mediterranean vegetation of Catalonia, Spain. Sci Total Environ 2004;329:241–59.
Parra R, Jimenez P, Baldasano JM. Development of the high spatial resolution EMICAT2000 emission model for air pollutants from the north-eastern Iberian Peninsula (Catalonia, Spain). Environ Pollut 2006;140:200–19.
Pay MT, Piot M, Jorba O, Basart S, Gassó S, Jiménez-Guerrero P, et al. A full year evaluation of the CALIOPE-EU air quality system in Europe for 2004: a model study. Atmos Environ 2010a. doi:10.1016/j.atmosenv.2010.050140.
Pay MT, Jiménez-Guerrero P, Baldasano JM. Implementation of resuspension from paved roads for the improvement of CALIOPE air quality system in Spain. Atmos Environ 2010b. doi:10.1016/j.atmosenv.2010.10.032.
Pénard-Morand C, Charpi D, Raherison C, Kopferschmitt C, Caillaud D, Lavaud F, et al. Long-term exposure to background air pollution related to respiratory and allergic health in schoolchildren. Clin Exp Allergy 2005;35(10):1279–87. doi:10.1111/j.1365-2222.2005.02336.
Pérez C, Nickovic S, Baldasano JM, Sicard M, Rocadenbosch F, Cachorro VE. A long Saharan dust event over the western Mediterranean: lidar, sun photometer observations, and regional dust modeling. J Geophys Res 2006a;111(D15214):1-16. doi:10.1029/2005JD006579.
Pérez C, Nickovic S, Pejanovic G, Baldasano JM, Ozsoy E. Interactive dust–radiation modeling: a step to improve weather forecasts. J Geophys Res 2006b;111(D16206). doi:10.1029/2005JD006717, 1–17.
Querol X, Alastuey A, Rodríguez S, Plana F, Ruiz CR, Cots N, et al. PM10 and PM2:5 source apportionment in the Barcelona metropolitan area, Catalonia, Spain. Atmos Environ 2001;35(36):6407–19.
Querol X, Alastuey A, Rodríguez S, Viana MM, Artiñano BA, Salvador P, et al. Estudio y evaluación de la contaminación atmosférica por material particulado en España: Informes finales. Technical Report. IJA CSIC, ISCIII, CIEMAT. Universidad de Huelva, Universidad del País Vasco; 2003.
Querol X, Alastuey A, Rodríguez S, Viana MM, Artiñano BA, Salvador P, et al. Levels of particulate matter in rural, urban and industrial sites in Spain. Sci Total Environ 2004a:334–5. doi:10.1016/j.scitotenv.2004.04.036. 359–376.
Querol X, Alastuey A, Ruiz CR, Artiñano B, Hansson HC, Harrison RM, et al. Speciation and origin of PM10 and PM2:5 in selected European cities. Atmos Environ 2004b;38:6547–55.
Querol X, Alastuey A, Moreno T, Viana MM, Castillo S, Pey J, et al. Spatial and temporal variations in airborne particulate matter (PM10 and PM2:5) across Spain 1999–2005. Atmos Environ 2008;42(17):396-3979. doi:10.1016/j.atmosenv.2006.10.071.
Rodríguez S, Querol X, Alastuey A, Plana F. Sources and processes affecting levels and composition of atmospheric aerosol in the western Mediterranean. J Geophys Res 2002;107(D24):4777.
Russell A, Dennis R. NARSTO critical review of photochemical models and modeling. Atmos Environ 2000;34(12–14):2283–324. doi:10.1016/S1352-2310(99)00468-9.
San José R, Rodriguez MA, Cortés E, González RM. Emma model: an advanced operational mesoscale air quality model for urban and regional environments. Environ Manage Health 1999;10(4):258–66.
Schell B, Ackermann IJ, Hass H, Binkowski FS, Ebel A. Modeling the formation of secondary organic aerosol within a comprehensive air quality model system. J Geophys Res 2001;106(D22):28275–93 2001JD000384.
Seinfeld JH, Pandis SN. Atmospheric chemistry and physics. New York, Chichester, Weinheim: John Wiley & Sons; 1998.
Skamarock WC, Klemp JB. A time-split nonhydrostatic atmospheric model for weather research and forecasting applications. J Comput Phys 2008;227(7):3465–85. doi:10.1016/j.jcp. 2007.01.037.
Smith SN, Mueller SF. Modeling natural emissions in the community multiscale air quality (CMAQ) model—part 1: building an emissions data base. Atmos Chem Phys Discuss 2010;10:1755–821.

Staudt M, Bertin N, Frenzel B, Seufert G. Seasonal variations in amount and composition of monoterpenes emitted by young Pinus pinea trees—implications for emission modeling. J Atmos Chem 2000;35:77–99.

Stein A, Mantilla E, Millán M. Using measured and modeled indicators to assess ozone-NO_x-VOC sensitivity in a western Mediterranean coastal environment. Atmos Environ 2005;39:7167–80.

Steinbrecher R, Smiatek G, Köble R, Seufert G, Thelokec J, Hauff K, et al. Intra- and inter-annual variability of VOC emissions from natural and semi-natural vegetation in Europe and neighbouring countries. Atmos Environ 2009;43:1380–91.

Talbot RW, Harriss RC, Browell EV, Gregory GL, Sebacher DI, Beck SM. Distribution and geochemistry of aerosols in the tropical north atlantic troposphere: relationship to Saharan dust. J Geophys Res 1986;91(D4):5173–82.

US-EPA. Interim procedures for evaluating air quality models (revised). Technical Report. EPA-450/4-91-013. Research Triangle Park, NC: U.S. Environmental Protection Agency, Office of Air Quality Planning and Standards; 1984.

US-EPA. Guideline for regulatory application of the urban airshed model. Technical Report. EPA-450/4-91-013. Research Triangle Park, NC: U.S. Environmental Protection Agency, Office of Air Quality Planning and Standards; 1991.

US-EPA, 2007. AP-42. 5th Edition, Volume VI, Chapter 13, Section 13.2.1. Paved Roads. Technical Report. U.S.-Environmental Protection Agency. US-EPA, 2007. Guidance on the Use of Models and Other Analyses for Demonstrating Attaintment of Air Quality Goals for Ozone, PM2.5, and Regional Haze. Technical Report. EPA-454/B-07-002. U.S. Environmental Protection Agency, Office of Air Quality Planning and Standards: Research Triangle Park, NC.

Vautard R, Bessagnet B, Chin M, Menut L. On the contribution of natural aeolian sources to particulate matter concentrations in Europe: testing hypotheses with a modelling approach. Atmos Environ 2005a;39(18):3291–303. doi:10.1016/j.atmosenv.2005.01.051.

Vautard R, Honoré C, Beekmann M, Rouïl L. Simulation of ozone during the august 2003 heat wave and emission control scenarios. Atmos Environ 2005b;39(16):2957–67. doi:10.1016/j.atmosenv.2005.01.039.

Venkatram A, Pleim J. The electrical analogy does not apply to modeling dry deposition of particles. Atmos Environ 1999;33(18):3075–6. doi:10.1016/S1352-2310(99)00094-1.

Viana M, Pérez C, Querol X, Alastuey A, Nickovic S, Baldasano JM. Spatial and temporal variability of PM levels and composition in a complex summer atmospheric scenario in Barcelona (NE Spain). Atmos Environ 2005;39:5343–61.

Vivanco MG, Correa M, Azula O, Palomino I, Martin F, Computer Science LN. Influence of model resolution on ozone predictions over Madrid area (Spain). Computational science and its applications ICCSA 2008. Heidelberg: Springer Berlin; 2008. p. 165–78.

Vivanco MG, Palomino I, Vautard R, Bessagnet B, Martín F, Menut L, et al. Multi-year assessment of photochemical air quality simulation over Spain. Environ Modell Softw 2009;24:63–73.

Weil JC, Sykes RI, Venkatram A. Evaluating air-quality models: review and outlook. J Appl Meteorol 1992;31:1121–45.

Zhang K, Knipping E, Wexler A, Bhave P, Tonnesen G. Size distribution of sea-salt emissions as a function of relative humidity. Atmos Environ 2005;39:3373–9.